ARTICLE

doi:10.1038/nature21693

Myeloid progenitor cluster formation drives emergency and leukaemic myelopoiesis

Aurélie Hérault[1]*, Mikhail Binnewies[1]*, Stephanie Leong[1]*, Fernando J. Calero-Nieto[2], Si Yi Zhang[1], Yoon-A Kang[1], Xiaonan Wang[2], Eric M. Pietras[1], S. Haihua Chu[3], Keegan Barry-Holson[1], Scott Armstrong[3], Berthold Göttgens[2] & Emmanuelle Passegué[1]†

Although many aspects of blood production are well understood, the spatial organization of myeloid differentiation in the bone marrow remains unknown. Here we use imaging to track granulocyte/macrophage progenitor (GMP) behaviour in mice during emergency and leukaemic myelopoiesis. In the steady state, we find individual GMPs scattered throughout the bone marrow. During regeneration, we observe expanding GMP patches forming defined GMP clusters, which, in turn, locally differentiate into granulocytes. The timed release of important bone marrow niche signals (SCF, IL-1β, G-CSF, TGFβ and CXCL4) and activation of an inducible *Irf8* and β-catenin progenitor self-renewal network control the transient formation of regenerating GMP clusters. In leukaemia, we show that GMP clusters are constantly produced owing to persistent activation of the self-renewal network and a lack of termination cytokines that normally restore haematopoietic stem-cell quiescence. Our results uncover a previously unrecognized dynamic behaviour of GMPs *in situ*, which tunes emergency myelopoiesis and is hijacked in leukaemia.

Our understanding of blood production has evolved considerably over the past years, mainly due to the introduction of new technologies to study haematopoietic stem cell (HSC) biology both *in situ* in their bone marrow (BM) niche and at the clonal level. Recent tracking approaches in native conditions, as opposed to transplantation experiments, have uncovered a prominent role for multipotent progenitors (MPPs) in maintaining blood production[1,2]. Detailed functional studies of the MPP compartment have identified three distinct MPP subsets (MPP2, MPP3 and MPP4) with unique lineage preferences that work together to adjust blood production to the needs of the organism[3,4]. In particular, increased production of myeloid-biased MPP2 and MPP3 by HSCs and myeloid reprogramming of lymphoid-biased MPP4 are now emerging as key first steps of regenerative myelopoiesis[4].

Myelopoiesis has long been considered to progress with the orderly differentiation of MPPs into uncommitted common myeloid progenitors, which then produce lineage-committed granulocyte/macrophage progenitors (GMPs) and megakaryocyte/erythrocyte progenitors[5]. Of note, single-cell RNA sequencing (RNA-seq) approaches[6,7] and more refined barcoding lineage-tracking experiments[8] indicate pre-existing lineage specifications in common myeloid progenitors, and a large degree of molecular and functional heterogeneity in all myeloid progenitor populations. However, our knowledge of myeloid progenitor biology still lacks a precise understanding of how myeloid differentiation occurs spatially in the BM cavity. Here, we used imaging approaches to provide insights into the mechanisms by which the BM niche microenvironment controls myelopoiesis.

Imaging GMPs *in situ*

We took advantage of the phenotypic characteristics of GMPs (Lin^- $c\text{-}Kit^+Sca\text{-}1^-Fc\gamma R^+CD34^+$)[5] to design an immunofluorescence staining scheme allowing their specific recognition on isolated populations and bone sections (Extended Data Fig. 1a). In wild-type mice, GMPs were scattered throughout the BM cavity with no particular distribution in relation to the bone endosteum, trabecular regions or central marrow, and were usually identified as individual cells intermingled with other haematopoietic populations (Fig. 1a). By contrast, in myeloproliferative neoplasm (MPN) models such as *Scl-tTA::TRE-BCR/ABL* (BA)[9] and $junB^{flox/flox}$*::MORE-cre* (jB)[10] mice, most GMPs were found as part of large, compact clusters surrounded by lineage-positive cells (Fig. 1b, Extended Data Fig. 1b, c). This process was progressive and directly associated with disease development, starting with loose GMP patches (pGMP) that evolved into large, compact GMP clusters (cGMP) (Extended Data Fig. 1d). We defined pGMPs as the collection of more than 4 GMPs loosely associated together, which could also be occasionally observed at steady state in wild-type mice, and distinguished them from cGMPs by the fact that they were not tightly surrounded by mature lineage cells (Extended Data Fig. 1e). While GMPs were never found in wild-type spleens, we observed abundant cGMPs in the disorganized red pulp of BA and jB mice (Extended Data Fig. 2a). Similar features were observed in the MLL-AF9 (MF9) transplanted model of acute myeloid leukaemia (AML)[11], with structures ranging from pGMPs to cGMPs (Extended Data Fig. 2b). Using a simplified version of this immunofluorescence scheme, we investigated whether cGMP formation was associated with a major re-organization of the BM microenvironment, but found no obvious changes in blood vessel network, hypoxia level, or deposition of extracellular matrix components, except for collagen IV as expected for the fibrotic BA mouse BM niche[12] (Extended Data Fig. 2c). We also localized mature populations in relation to cGMPs, and although some lymphoid cells were detected inside and at the periphery of cGMPs, myeloid cells were only found tightly surrounding cGMPs (Extended Data Fig. 2d). These results indicate that leukaemic myelopoiesis is characterized by the presence of cGMPs, which are part of a continuum of differentiation separating progenitors from mature myeloid cells.

[1]The Eli and Edythe Broad Center of Regeneration Medicine and Stem Cell Research, Department of Medicine, Division of Hematology/Oncology, University of California San Francisco, San Francisco, California 94143, USA. [2]Cambridge University Department of Haematology, Cambridge Institute for Medical Research, Wellcome Trust and MRC Cambridge Stem Cell Institute, Hills Road, Cambridge CB2 0XY, UK. [3]Department of Pediatric Oncology, Dana-Farber Cancer Institute, and Division of Hematology/Oncology, Boston Children's Hospital, Harvard Medical School, Boston, Massachusetts 02215, USA. †Present address: Columbia Stem Cell Initiative, Department of Genetics and Development, Columbia University Medical Center, New York, New York 10032, USA.
*These authors contributed equally to this work.

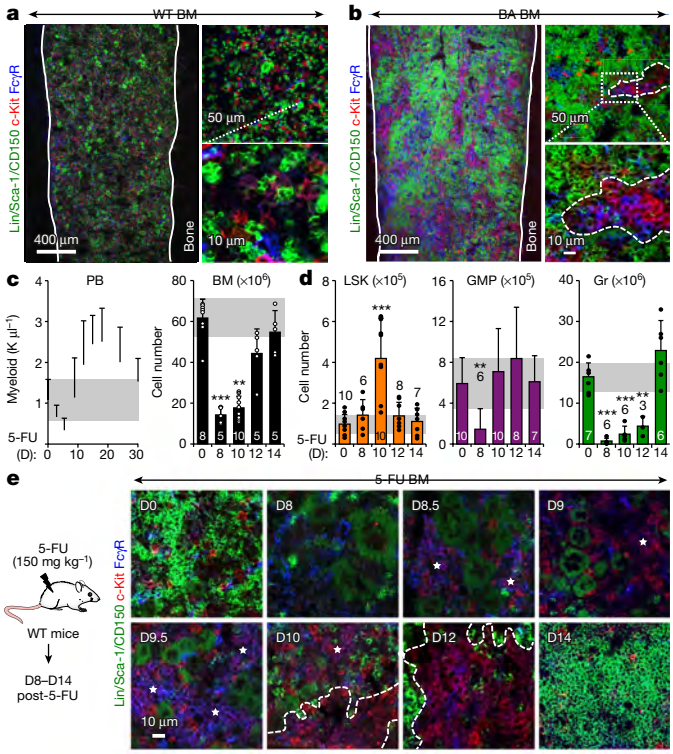

Figure 1 | GMP clusters in leukaemic and regenerative myelopoiesis. **a**, **b**, Representative immunofluorescence staining showing GMPs (purple) in the BM of wild-type (WT) (**a**) and diseased *Scl-tTA::TRE-BCR/ABL* (BA) (**b**) mice. Solid lines indicate bone surface, dotted lines denote cGMPs, and arrowheads indicate individual GMPs. **c**, Peripheral blood (PB) ($n = 5$) and BM regeneration in 5-FU-treated wild-type mice. D, day. **d**, Changes in haematopoietic populations at the indicated days after 5-FU treatment. Gr, granulocytes. **e**, Representative immunofluorescence staining showing GMPs (purple) in the BM of 5-FU-treated wild-type mice. Stars indicate pGMPs and dotted lines denote cGMPs. Data are mean ± s.d. (grey bars, reference range). $^{**}P < 0.01$, $^{***}P < 0.001$ (Student's *t*-test).

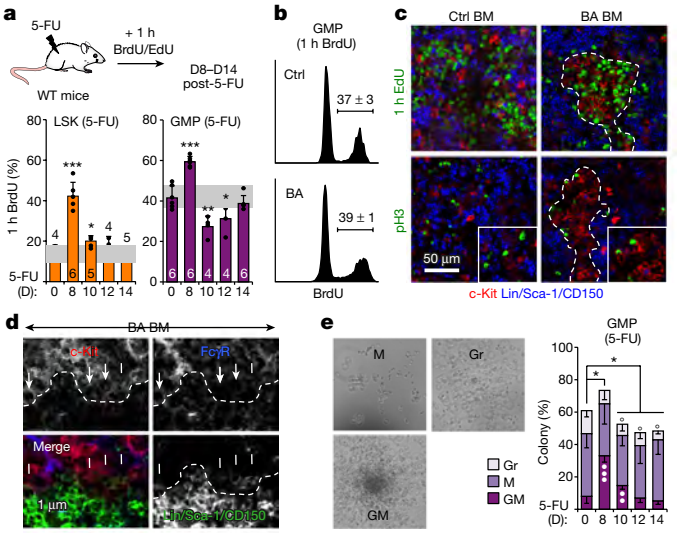

Figure 2 | GMP clusters are foci of differentiation. **a**, Proliferation in 5-FU-treated wild-type mice showing experimental scheme and BrdU/EdU incorporation in LSK cells and GMPs ($n = 3$). **b**, BrdU incorporation in GMPs from control (Ctrl) and BA mice ($n = 3$). **c**, Representative immunofluorescence staining showing myeloid progenitors (red) in relation to proliferating EdU$^+$ (green, top) and dividing pH3$^+$ (green, bottom) cells in BM from control and BA mice. **d**, Representative staining of GMP cluster periphery (dotted lines), highlighting differentiating GMPs (arrows) as they lose FcγR expression and gain lineage marker expression. **e**, Single-cell clonogenic methylcellulose analyses of GMPs isolated from 5-FU-treated wild-type mice ($n = 4$). Results are percentage of colony types (asterisks denote significance versus day 0 plating efficiency; filled circles versus granulocyte/macrophage colonies; open circles versus macrophage colonies), and pictures show representative colonies (GM, granulocyte/macrophages; M, macrophages). Dotted lines denote cGMPs. Data are mean ± s.d. (grey bars, reference range). $^{*}P \leq 0.05$, $^{**}P \leq 0.01$, $^{***}P \leq 0.001$ (Student's *t*-test).

cGMPs are features of myeloid expansion

To determine whether cGMPs could be detected during emergency myelopoiesis, we used several models of myeloid regeneration or active myeloid cell production. First, wild-type mice were injected once with 5-fluorouracil (5-FU; 150 mg kg^{-1}) and followed for myeloid regeneration over time (Fig. 1c). Flow cytometry analyses showed increased numbers of immature Lin$^-$c-Kit$^+$Sca-1$^+$ (LSK) cells by day 10, which essentially reflected increased production of myeloid-biased MPP2 and MPP3 by 5-FU-activated HSCs (Fig. 1d, Extended Data Fig. 3a, b). By contrast, GMP numbers were reduced by day 8 and reverted to steady-state levels by day 10, whereas granulocyte numbers sharply decreased by day 8, and then slowly recovered to exceed steady-state levels by day 14. Notably, immunofluorescence staining of 5-FU-treated BM showed rare GMPs at day 8, followed by the appearance of pGMPs by day 8.5, which quickly expanded in size up to day 10 when the first cGMPs were observed (Fig. 1e, Extended Data Fig. 3c). By day 12, we only found cGMPs, particularly along the bone endosteum, which then had completely disappeared by day 14 upon granulocyte restoration. We observed similar transient cGMP formation in wild-type mice injected once with Ly-6G antibody (0.1 mg per mouse) to ablate granulocytes specifically[13], or daily with G-CSF (5 μg per mouse) to increase granulocyte production[14] (Extended Data Fig. 4a, b). We also confirmed transient cGMP formation during the peak of myeloid regeneration after HSC transplantation, when both myeloid-biased MPP2/MPP3 and GMPs were specifically expanded[4] (Extended Data Fig. 4c). Moreover, we demonstrated that cGMPs were predominantly clonal and composed of GMPs derived from individual HSCs undergoing regenerative or leukaemic myelopoiesis (Supplementary Information, Extended Data Fig. 5a–d). Collectively, these results indicate that transient cGMP formation is a hallmark characteristic of emergency myelopoiesis.

cGMPs are foci of myeloid differentiation

To understand the mechanisms of cGMP formation, we conducted detailed cell cycle analyses by injecting BrdU or EdU into 5-FU-treated wild-type mice (Fig. 2a, Extended Data Fig. 6a, b). In LSK cells, BrdU incorporation peaked at day 8 and then progressively reverted to steady-state levels by day 12. In GMPs, BrdU incorporation first increased at day 8, at the onset of pGMP formation, and then dropped below steady-state levels between days 10 and 12 when pGMPs turned into cGMPs, before reverting to steady-state levels by day 14 when cGMPs had disappeared. This pattern was reflected in immunofluorescence staining, with proliferating EdU$^+$ pGMPs observed at day 10, and cGMPs markedly devoid of proliferating EdU$^+$ cells compared to their surroundings at day 12. By contrast, the number of dividing phospho-histone H3 (pH3)-positive myeloid progenitors was not different between cGMPs and their surroundings at days 10–12, although they appeared preferentially located along the edges of the clusters. Similar analyses performed in BA mice did not uncover altered GMP proliferation rates, and emphasized the preferential distribution of pH3$^+$ dividing cells along the edges of the clusters (Fig. 2b, c). Close examination of the cGMP periphery in BA mice highlighted a clear differentiation gradient, with reciprocal expression patterns for FcγR and lineage markers in GMPs undergoing differentiation across the cluster boundary defined by c-Kit expression (Fig. 2d). Single-cell clonogenic methylcellulose analyses of GMPs isolated from 5-FU-treated wild-type mice confirmed a change in differentiation

potential associated with cGMP formation, with increased plating efficiency and immature granulocyte/macrophage colonies at days 8–10, followed by restoration of low granulocyte/macrophage frequency and a significant loss of macrophage colonies at days 12–14 (Fig. 2e). We also confirmed that mature myeloid cells also directly surrounded cGMPs in 5-FU-treated mice (Extended Data Fig. 6c). Collectively, these results uncover complex changes in the cellular behaviour of GMPs associated with cluster formation, with increased proliferation and immaturity in expanding pGMPs that form cGMPs, followed by a sharp block in proliferation and restoration of the differentiation potential in differentiating cGMPs that divide to produce mature granulocytes. Moreover, these features of cGMPs as foci of differentiation appear conserved during leukaemic myelopoiesis.

Molecular reprograming in cGMPs

To gain insights into the molecular mechanism controlling cGMP formation, we investigated pools of 100 GMPs isolated from 5-FU-treated wild-type mice using a custom-made Fluidigm quantitative reverse transcription PCR (qRT–PCR) array (Supplementary Table 1). Principal component and *t*-distributed stochastic neighbour embedding (tSNE) analyses of the 59 most robustly expressed genes revealed two distinct groups, with day 8 and most day 10 samples (group I) clearly separated from samples from day 0 and days 12–14 (group II) (Fig. 3a). Examination of individual genes highlighted signatures of activated cell cycle and strong molecular immaturity in expanding pGMPs (group I), which were completely reverted in differentiating cGMPs (group II) (Fig. 3b, Extended Data Fig. 7a–c). Similar investigations with leukaemic GMPs revealed a molecular signature of expanding pGMPs in GMPs from both BA and jB mice, with increased *Ccne1* expression and decreased levels of *Irf8*, *Csf1r* (also known as *M-CSFR*) and *Il6ra* (Fig. 3c, Extended Data Fig. 7d, Supplementary Table 2). To investigate global transcriptional changes, we also performed single-cell RNA-seq on GMPs isolated from 5-FU-treated wild-type mice, and BA and age-matched control mice. Principal component analysis and hierarchical clustering of all single GMPs also displayed two major clusters (Fig. 3d, Extended Data Fig. 7e, Supplementary Tables 3 and 4). Remarkably, day 0 and control GMPs showed high expression of the previously defined group II genes and reflected steady-state GMPs, whereas day 8 5-FU-treated and BA GMPs were characterized by expression of group II genes and coincided with self-renewing GMPs. Allocation to each cluster of all single GMPs across the 5-FU kinetics and in BA mice showed the presence of 8.5–13.5% self-renewing GMPs at the steady state, and persistence of around 15% of steady-state GMPs at day 8 and the peak of self-renewing pGMPs (Fig. 3e). Together, these results uncover considerable molecular reprogramming during cGMP formation, characterized by cell cycle activation and suppression of maturation pathways in expanding pGMPs, followed by cell cycle blockade and re-activation of maturation pathways in differentiating cGMPs. They also indicate that leukaemic GMPs are molecularly primed for cGMP formation. Moreover, they demonstrate the co-existence of distinct steady-state and self-renewing GMPs in both normal and leukaemic contexts, in proportions that reflect the activation state of emergency myelopoiesis.

GMP self-renewal network

We next probed the function of the key myeloid transcription factor *Irf8* (ref. 15) in cGMP formation. *Irf8*$^{-/-}$ mice are immunodeficient and develop MPN over time[16]. Similar to BA and jB mice, we observed constitutive cGMP formation in the BM of primary or transplanted *Irf8*$^{-/-}$ mice (Fig. 4a, Extended Data Fig. 8a–c), thus demonstrating that decreasing *Irf8* expression is sufficient to drive cGMP formation. We also found delayed cGMP formation in 5-FU-treated primary and transplanted *Irf8*$^{-/-}$ mice, which, in turn, indicates that restoration of *Irf8* expression is essential for cGMP differentiation, probably by increasing expression of genes such as *Csf1r*, a direct *Irf8* target[17]. Notably, *Irf8* and *Ctnnb1* (encoding β-catenin) are part of an antagonistic regulatory

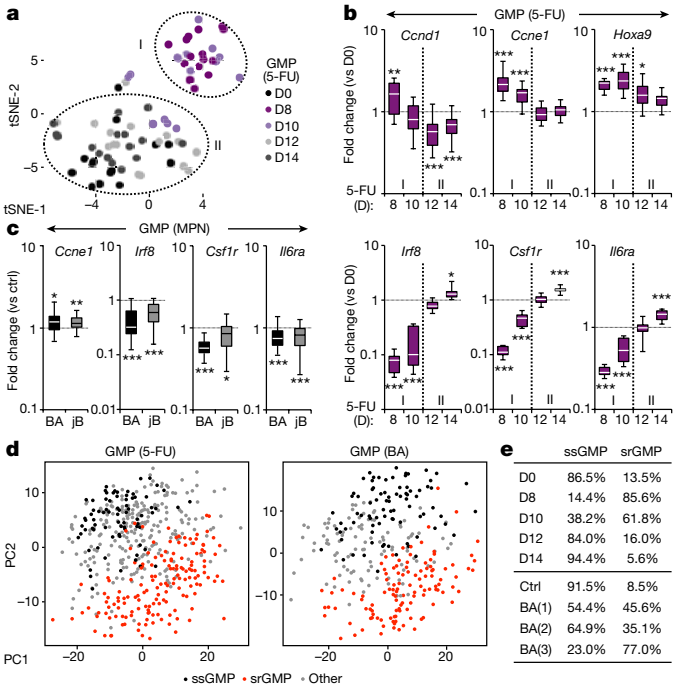

Figure 3 | Molecular mechanisms of GMP cluster formation. a, tSNE analyses of Fluidigm gene expression data from GMPs isolated from 5-FU-treated wild-type mice ($n = 2$; 10–16 pools of 100 cells per condition). **b**, Selected genes from Fluidigm analyses shown in **a**. Results are expressed as fold change compared to levels in day 0 GMPs and presented as boxplots (line: median; box: twenty-fifth and seventy-fifth percentiles; whisker: ninetieth and tenth percentiles). **c**, Selected genes from Fluidigm analyses of GMPs isolated from BA, jB and respective age-matched control mice ($n = 4$; 22–28 pools of 100 cells per condition). Results are expressed as fold change compared to levels in respective control GMPs and presented as in **b**. **d**, Principal component (PC) analyses of single-cell RNA-seq data from GMPs isolated from 5-FU-treated wild-type (476 single cells) and BA (306 single cells) mice. **e**, Frequency of steady-state GMPs (ssGMP) and self-renewing GMPs (srGMP) in 5-FU-treated wild-type mice, and control and BA mice. $^{*}P \leq 0.05$, $^{**}P \leq 0.01$, $^{***}P \leq 0.001$ (Student's *t*-test).

network in chronic myeloid leukaemia (CML)[18], and activated β-catenin signalling provides aberrant self-renewal features to leukaemic GMPs in both CML and AML[19,20]. Notably, we observed increased levels of nuclear β-catenin in day 8 regenerating GMPs, and in GMPs from both BA and jB mice (Fig. 4b, c). However, downregulation of *Irf8* did not directly drive β-catenin as neither *Irf8*$^{-/-}$ GMPs nor HSCs or MPPs showed increased nuclear β-catenin (Fig. 4d, Extended Data Fig. 8d). By contrast, GMPs from *Ctnnb1* gain-of-function (GOF) and loss-of-function (LOF) mice had decreased and increased *Irf8* expression, respectively, leading to the presence of pGMPs at the steady state in *Ctnnb1* GOF mice, and unchanged steady-state levels but delayed cGMP formation after 5-FU treatment in *Ctnnb1* LOF mice (Fig. 4e–g, Extended Data Fig. 8e, f). Collectively, these results place *Irf8* and β-catenin at the centre of an inducible self-renewal progenitor network controlling cGMP formation, with β-catenin directly suppressing *Irf8* expression and *Irf8* eventually re-enforcing β-catenin expression in MPN contexts (Fig. 4h).

BM niche signals control cGMP formation

To identify the environmental factors involved in cGMP formation, we performed ELISA analyses on BM fluid from 5-FU-treated wild-type mice (Fig. 5a). Notably, we found significantly increased levels of cytokines known to stimulate HSC proliferation and trigger myeloid differentiation, such as SCF, G-CSF and IL-1, before pGMP expansion (days 5–8), and factors important for restoring HSC quiescence, such as

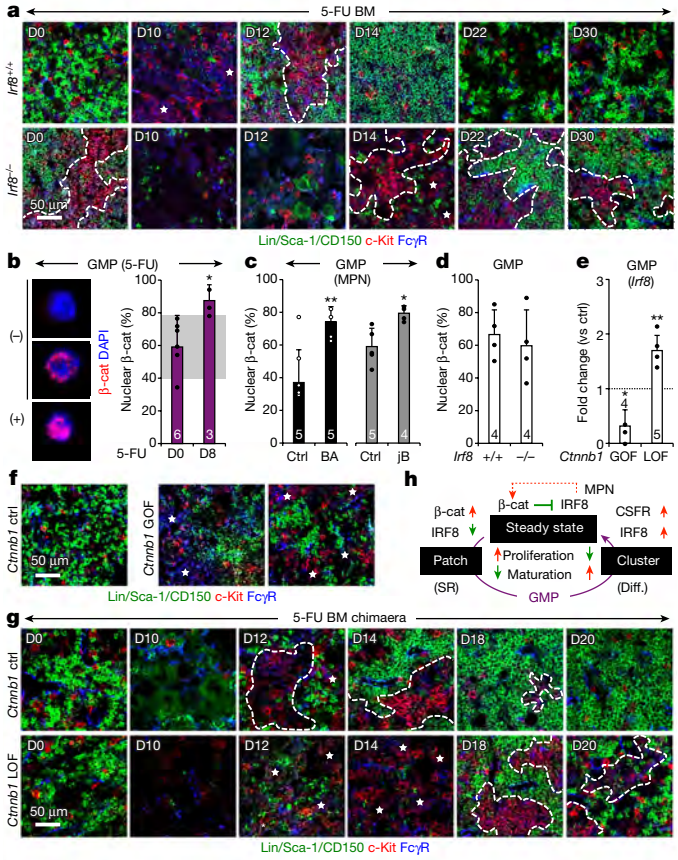

Figure 4 | *Irf8* and β-catenin self-renewal progenitor network. **a**, Representative immunofluorescence staining of GMPs (purple) in BM from 5-FU-treated *Irf8*$^{+/+}$ and *Irf8*$^{-/-}$ mice. **b**–**d**, Nuclear β-catenin expression in GMPs from day 8 5-FU-treated wild-type mice with representative negative (−) and positive (+) staining shown for day 0 GMPs (**b**), GMPs from BA, jB and respective age-matched control mice (**c**), and GMPs from *Irf8*$^{+/+}$ and *Irf8*$^{-/-}$ mice (**d**). Results are expressed as the percentage of positive cells. **e**, *Irf8* expression in GMPs from *Ctnnb1* gain-of-function (GOF) and loss-of-function (LOF) mice (dotted line, control level). **f**, Representative staining of GMPs (purple) in BM from *Ctnnb1* control and GOF mice. **g**, Representative staining of GMPs (purple) in BM from 5-FU-treated *Ctnnb1* control and LOF mice. **h**, Model of the molecular network controlling pGMP self-renewal (SR) and cGMP differentiation (diff.). Red indicates activation; green denotes suppression; and dotted line highlights re-enforcing pathways in MPN. In all images, stars indicate pGMPs and dotted lines denote cGMPs. Data are mean ± s.d. (grey bars, reference range). *$P \leq 0.05$, **$P \leq 0.01$ (Student's *t*-test).

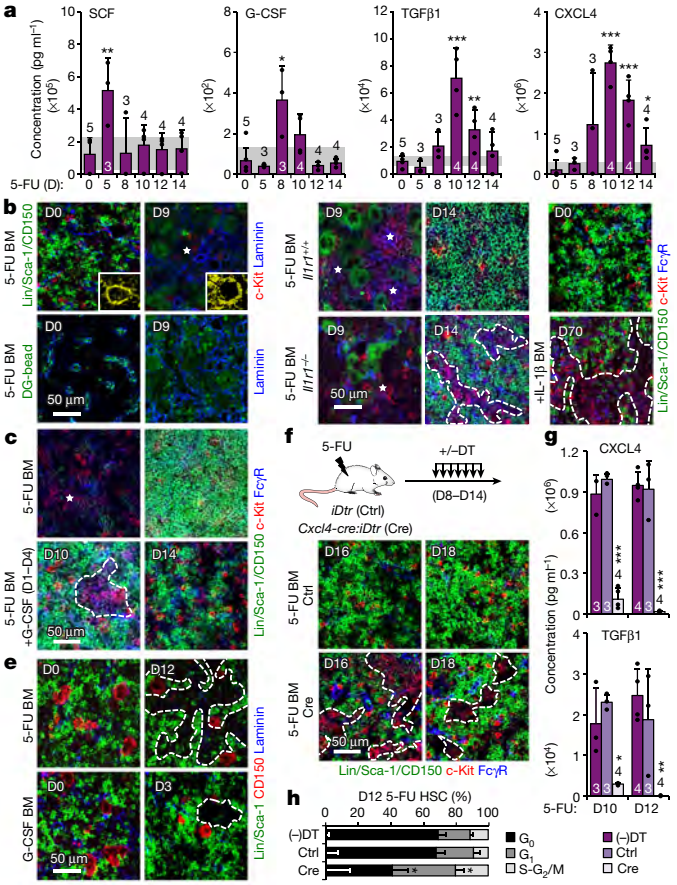

Figure 5 | BM niche controls of GMP cluster formation during regenerative myelopoiesis. **a**, ELISA cytokine measurements in BM fluids of 5-FU-treated wild-type mice ($n = 3$). **b**, Representative immunofluorescence staining showing vasculature (blue, pseudo-coloured in yellow in magnified inserts) and vascular leakage (green, dragon-green (DG) beads) in BM from 5-FU-treated mice. **c**, Representative staining showing GMPs (purple) in BM from 5-FU-treated mice, with or without concomitant daily injections of G-CSF on days 1 to 4. **d**, Representative staining of GMPs (purple) in *Il1r1*$^{+/+}$ and *Il1r1*$^{-/-}$ 5-FU-treated BM, or BM of IL-1β-injected wild-type mice. **e**, Representative staining showing CD150^{+} megakaryocytes (red) in 5-FU- and G-CSF-treated wild-type BM. **f**–**h**, Megakaryocyte depletion studies in diphtheria toxin (DT)-injected *iDtr* (control) and *Cxcl4-cre:iDtr* (Cre) mice, and non-injected control mice (−DT). **f**, Experimental scheme and representative immunofluorescence staining of GMPs (purple) in BM from 5-FU-treated mice. **g**, ELISA cytokine measurements in BM fluids at day 10 ($n = 3$) and day 12 ($n = 4$). **h**, HSC cell cycle distribution at day 12 ($n = 3$). In all images, stars indicate pGMPs and dotted lines denote cGMPs. Data are mean ± s.d. (grey bars, reference range). *$P \leq 0.05$; **$P \leq 0.01$, ***$P \leq 0.001$ (Student's *t*-test).

TGFβ1 and CXCL4 (also known as PF4), at the time of cGMP formation (days 10–12)[21]. By contrast, we observed no change in the BM homing chemokine CXCL12 (also known as SDF1α), and a decrease rather than the reported increase[22] in FGF1 production (Extended Data Fig. 9a). G-CSF and IL-1 are both produced by the damaged vasculature in stress conditions[13,23]. Immunofluorescence staining confirmed notable vascular damage after 5-FU treatment, with major gaps between dysmorphic laminin^{+} endothelial cells leading to vascular leakage into the stromal microenvironment, especially at days 8–10 when pGMPs expand (Fig. 5b, Extended Data Fig. 9b). To probe the role of G-CSF directly, we injected it for 4 consecutive days in 5-FU-treated wild-type mice either from days 1 to 4 (early injections) before pGMP expansion, or from days 8 to 11 (late injections) during the cGMP differentiation period (Fig. 5c, Extended Data Fig. 9c). Notably, early G-CSF injections markedly accelerated cGMP formation, whereas late G-CSF injections considerably amplified and extended the period of cGMP formation. In addition, we recently reported impaired myeloid regeneration in 5-FU-treated *Il1r1*$^{-/-}$ mice, and showed that IL-1 triggers regenerative myelopoiesis by activating PU.1 in HSCs[23]. Consistently, we observed markedly delayed cGMP formation in 5-FU-treated *Il1r1*$^{-/-}$ mice, and constitutive cGMP formation at the steady state in IL-1-treated wild-type mice (Fig. 5d, Extended Data Fig. 9d).

TGFβ1 and CXCL4 are both produced by megakaryocytes, which are important components of the HSC niche[24,25]. Immunofluorescence staining showed an overabundance of large, mature CD150^{+} megakaryocytes in close association with cGMPs in every tested regenerative context, including 5-FU, G-CSF and Ly-6G treatments (Fig. 5e, Extended Data Fig. 9e). To address the role of megakaryocytes in secreting quiescence-enforcing signals, we used a previously published diphtheria-toxin-based approach to deplete megakaryocytes in 5-FU-treated *Cxcl4-cre::iDtr* mice[24] (Fig. 5f, Extended Data Fig. 9f). Remarkably, megakaryocytes depletion caused persisting cGMP

formation during the granulocyte outburst period, a massive reduction in CXCL4 and TGFβ1 production, and prevention of HSC return to quiescence (Fig. 5f–h, Extended Data Fig. 9g). Collectively, these findings demonstrate that many distinct and temporally regulated BM niche signals are important for various aspects of cGMP formation (Fig. 6a). This includes the early production of SCF and IL-1, which activate HSCs to produce MPP2/MPP3 and initiate emergency myelopoiesis, the release of G-CSF, which dictates when self-renewing pGMPs are formed, probably by triggering the *Irf8* and β-catenin progenitor self-renewal network, and the late production of TGFβ1 and CXCL4 by megakaryocytes surrounding cGMPs, which re-establish HSC quiescence and limit the duration of the regenerative response.

Deregulated cGMP formation in leukaemia

To understand why cGMP formation is constitutively activated in leukaemia, we performed similar ELISA analyses on BM fluid from BA and jB mice (Fig. 6b, Extended Data Fig. 10a). Notably, we found a consistent decrease in quiescence-enforcing cytokines in both MPN models, with undetectable levels of TGFβ1 and CXCL4 in BA mice, and significantly reduced TGFβ1 production in jB mice. Immunofluorescence staining revealed decreased numbers of CD150$^+$ megakaryocytes in close proximity of cGMPs in both MPN models, ranging from almost absent in BA mice to infrequent in jB mice (Fig. 6c). qRT–PCR analyses further confirmed reduced *Cxcl4* (also known as *Pf4*) expression from BA megakaryocytes (Extended Data Fig. 10b). Moreover, immunofluorescence of laminin$^+$ blood vessels indicated constitutively damaged endothelial cells with high vascular leakage in both MPN models (Fig. 6c, Extended Data Fig. 10c). We also observed persistence of very large cGMPs associated with constant granulocyte overproduction in 5-FU-treated BA mice (Fig. 6d, Extended Data Fig. 10d). These results indicate that transformed HSC-derived leukaemic stem cells continuously produce cGMPs as a direct consequence of high levels of activating cytokines, such as IL-1, produced by the inflamed leukaemic BM niche[12]. This, in turn, results in the overproduction of MPP2 and MPP3 (ref. 9), which are committed to form pGMPs probably because of to the constitutive activation of the progenitor self-renewal *Irf8* and β-catenin network by the driving oncogenes, rather than by extrinsic myeloid cytokines. Most importantly, this activation process never stops because essential quiescence-enforcing cytokines such as TGFβ1 and CXCL4 are missing owing to the loss or insufficient production of leukaemic megakaryocytes. Altogether, these results demonstrate that the leukaemic BM niche is both constitutively activated and lacking important feedback mechanisms, thereby driving constant cGMP formation and granulocyte production (Fig. 6e).

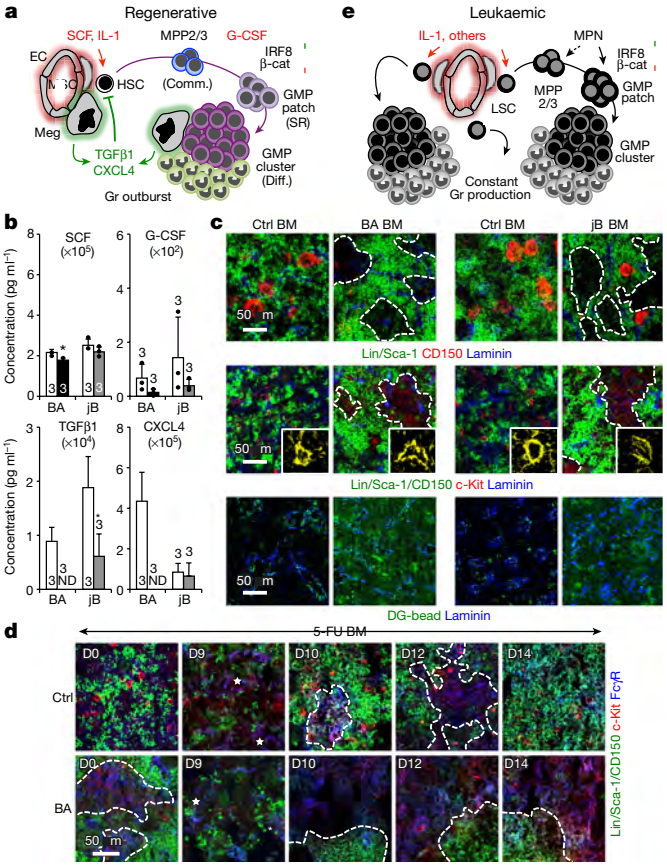

Figure 6 | Continuous GMP cluster formation in leukaemic myelopoiesis. **a**, Model of regenerative myelopoiesis. Comm., commitment; EC, endothelial cells; Meg, megakaryocytes; MSC, mesenchymal stromal cells. Red indicates activation, green denotes suppression. **b**, ELISA cytokine measurements in BM fluids of diseased BA (black), jB (grey) and respective control (white) mice ($n = 3$; ND, not detected). **c**, Representative immunofluorescence staining showing CD150$^+$ megakaryocytes (red), vasculature (blue, pseudo-coloured in yellow in magnified inserts) and vascular leakage (green, dragon-green (DG) bead) in BM from BA, jB and respective control mice. **d**, Representative immunofluorescence staining of GMPs (purple) in BM from 5-FU-treated control and BA mice. **e**, Model of leukaemic myelopoiesis. LSC, leukaemia-initiating stem cells. Stars indicate pGMPs and dotted lines denote cGMPs. Data are mean ± s.d. $^*P \leq 0.05$ (Student's *t*-test).

Discussion

Our results expand the understanding of myeloid progenitor biology, and report a new and highly dynamic *in situ* behaviour of GMPs that link changes in their molecular and cellular functions with spatial organization in the BM niche. We identify two functional states for GMPs, with self-renewing pGMPs building GMP clusters, and differentiating cGMPs producing mature myeloid cells until the complete disappearance of the GMP clusters. This biphasic process is a transient feature of emergency myelopoiesis, and is highly controlled by the timed released of various BM niche signals. These findings, together with the recent identification of myeloid-biased MPP2 and MPP3 (ref. 4), help to construct a revised map of emergency myelopoiesis pathways and a deeper understanding of their hijacking in leukaemia (Extended Data Fig. 10e). They also provide an explanation for the recently reported molecular heterogeneity in GMPs[6,7,26], with the co-existence in variable proportions of distinct steady-state and self-renewing GMPs, and are essential for interpreting the results of lineage-tracking experiments showing major contributions of MPPs and myeloid progenitors to myeloid output[1,2]. Moreover, they equate cGMP formation with regulated myelopoiesis, and identify several mechanisms that could be harnessed for translational applications. Pathological investigations have reported the presence of immature myeloid cell aggregates in the bones of patients with leukaemia[27], including clusters of proliferating myeloblasts surrounded by TGFβ1-producing megakaryocytes[28], which could represent similar cGMP formation in humans. Future studies will address whether targeting various regulators of cGMP formation can be used to prevent the development of myeloid malignancies or, conversely, to boost myeloid cell production in myelosuppressed conditions.

Online Content Methods, along with any additional Extended Data display items and Source Data, are available in the online version of the paper; references unique to these sections appear only in the online paper.

Received 16 February 2016; accepted 7 February 2017.
Published online 29 March 2017.

1. Sun, J. *et al.* Clonal dynamics of native haematopoiesis. *Nature* **514,** 322–327 (2014).
2. Busch, K. *et al.* Fundamental properties of unperturbed haematopoiesis from stem cells *in vivo*. *Nature* **518,** 542–546 (2015).
3. Cabezas-Wallscheid, N. *et al.* Identification of regulatory networks in HSCs and their immediate progeny via integrated proteome, transcriptome, and DNA methylome analysis. *Cell Stem Cell* **15,** 507–522 (2014).

4. Pietras, E. M. *et al.* Functionally distinct subsets of lineage-biased multipotent progenitors control blood production in normal and regenerative conditions. *Cell Stem Cell* **17,** 35–46 (2015).
5. Akashi, K., Traver, D., Miyamoto, T. & Weissman, I. L. A clonogenic common myeloid progenitor that gives rise to all myeloid lineages. *Nature* **404,** 193–197 (2000).
6. Wilson, N. K. *et al.* Combined single-cell functional and gene expression analysis resolves heterogeneity within stem cell populations. *Cell Stem Cell* **16,** 712–724 (2015).
7. Paul, F. *et al.* Transcriptional heterogeneity and lineage commitment in myeloid progenitors. *Cell* **163,** 1663–1677 (2015).
8. Perié, L., Duffy, K. R., Kok, L., de Boer, R. J. & Schumacher, T. N. The branching point in erythro-myeloid differentiation. *Cell* **163,** 1655–1662 (2015).
9. Reynaud, D. *et al.* IL-6 controls leukemic multipotent progenitor cell fate and contributes to chronic myelogenous leukemia development. *Cancer Cell* **20,** 661–673 (2011).
10. Passegué, E., Wagner, E. F. & Weissman, I. L. JunB deficiency leads to a myeloproliferative disorder arising from hematopoietic stem cells. *Cell* **119,** 431–443 (2004).
11. Krivtsov, A. V. *et al.* Transformation from committed progenitor to leukaemia stem cell initiated by MLL-AF9. *Nature* **442,** 818–822 (2006).
12. Schepers, K. *et al.* Myeloproliferative neoplasia remodels the endosteal bone marrow niche into a self-reinforcing leukemic niche. *Cell Stem Cell* **13,** 285–299 (2013).
13. Cain, D. W., Snowden, P. B., Sempowski, G. D. & Kelsoe, G. Inflammation triggers emergency granulopoiesis through a density-dependent feedback mechanism. *PLoS One* **6,** e19957 (2011).
14. Boettcher, S. *et al.* Endothelial cells translate pathogen signals into G-CSF-driven emergency granulopoiesis. *Blood* **124,** 1393–1403 (2014).
15. Tamura, T., Kurotaki, D. & Koizumi, S. Regulation of myelopoiesis by the transcription factor IRF8. *Int. J. Hematol.* **101,** 342–351 (2015).
16. Holtschke, T. *et al.* Immunodeficiency and chronic myelogenous leukemia-like syndrome in mice with a targeted mutation of the *ICSBP* gene. *Cell* **87,** 307–317 (1996).
17. Scheller, M. *et al.* Altered development and cytokine responses of myeloid progenitors in the absence of transcription factor, interferon consensus sequence binding protein. *Blood* **94,** 3764–3771 (1999).
18. Scheller, M. *et al.* Cross talk between Wnt/β-catenin and Irf8 in leukemia progression and drug resistance. *J. Exp. Med.* **210,** 2239–2256 (2013).
19. Jamieson, C. H. *et al.* Granulocyte-macrophage progenitors as candidate leukemic stem cells in blast-crisis CML. *N. Engl. J. Med.* **351,** 657–667 (2004).
20. Wang, Y. *et al.* The Wnt/β-catenin pathway is required for the development of leukemia stem cells in AML. *Science* **327,** 1650–1653 (2010).
21. Schepers, K., Campbell, T. B. & Passegué, E. Normal and leukemic stem cell niches: insights and therapeutic opportunities. *Cell Stem Cell* **16,** 254–267 (2015).
22. Zhao, M. *et al.* Megakaryocytes maintain homeostatic quiescence and promote post-injury regeneration of hematopoietic stem cells. *Nat. Med.* **20,** 1321–1326 (2014).
23. Pietras, E. M. *et al.* Chronic interleukin-1 exposure drives haematopoietic stem cells towards precocious myeloid differentiation at the expense of self-renewal. *Nat. Cell Biol.* **18,** 607–618 (2016).
24. Bruns, I. *et al.* Megakaryocytes regulate hematopoietic stem cell quiescence through CXCL4 secretion. *Nat. Med.* **20,** 1315–1320 (2014).
25. Nakamura-Ishizu, A., Takubo, K., Kobayashi, H., Suzuki-Inoue, K. & Suda, T. CLEC-2 in megakaryocytes is critical for maintenance of hematopoietic stem cells in the bone marrow. *J. Exp. Med.* **212,** 2133–2146 (2015).
26. Olsson, A. *et al.* Single-cell analysis of mixed-lineage states leading to a binary cell fate choice. *Nature* **537,** 698–702 (2016).
27. Orazi, A. Histopathology in the diagnosis and classification of acute myeloid leukemia, myelodysplastic syndromes, and myelodysplastic/myeloproliferative diseases. *Pathobiology* **74,** 97–114 (2007).
28. Raza, A. *et al.* High expression of transforming growth factor-β long cell cycle times and a unique clustering of S-phase cells in patients with acute promyelocytic leukemia. *Blood* **79,** 1037–1048 (1992).

Supplementary Information is available in the online version of the paper.

Acknowledgements We thank A. Leavitt (UCSF) for providing G-CSF; P. Frenette for advice on imaging approaches and the gift of *Cxcl4-cre:iDTR* mice; M. Kissner and M. Lee for management of our Flow Cytometry core facility; and all members of the Passegué laboratory for critical insights and suggestions. This work was supported by NIH K01DK098315 award to E.M.P.; a Bloodwise and CRUK program grants and Wellcome Trust funding to the Cambridge Stem Cell Institute to B.G.; and NIH R01HL092471, R01HL111266 and P30DK063720 grants, Rita Allen Scholar Award and Leukemia Lymphoma Society Scholar Award to E.P.

Author Contributions A.H., M.B. and S.L. performed all of the experiments with help from S.Y.Z. for dragon bead assays, Y.-A.K. for β-catenin studies, E.M.P. for IL-1 experiments, F.J.C.-N., X.W. and B.G. for Fluidigm and single-cell RNA-seq analyses, and S.H.C. and S.A. for MLL/AF9 experiments. K.B.-H. initiated the imaging studies. A.H., M.B. and S.L. designed the experiments and interpreted the results. A.H. and E.P. wrote the manuscript.

Author Information Reprints and permissions information is available at www.nature.com/reprints. The authors declare no competing financial interests. Readers are welcome to comment on the online version of the paper. Publisher's note: Springer Nature remains neutral with regard to jurisdictional claims in published maps and institutional affiliations. Correspondence and requests for materials should be addressed to E.P. (ep2828@cumc.columbia.edu).

METHODS

Mice. Six- to twelve-week-old C57Bl/6-CD45.2 wild-type mice were used as donor for cell isolation and *in vivo* treatments. Eight- to twelve-week old C57Bl/6-CD45.1 (Boy/J) wild-type mice were used as recipients for cell transplantation experiments. C57Bl/6-CD45.2 *Scl-tTA::TRE-BCR/ABL* (BA)[9], *junB*$^{flox/flox}$*::MORE-Cre* (jB)[10], *Irf8*$^{-/-}$ [16], *Il1r1*$^{-/-}$ [29], *Csf1r-Gfp*[30], *Actb-Gfp*[31], *Ctnnb1 Flox(Ex3)* (GOF)[32], *Ctnnb1*$^{flox/flox}$ (LOF)[33], *Mx1-cre*[34], *Cxcl4-cre*[35] and *iDtr*[36] mice were used for bone collection and *in vivo* treatments at various ages. Bones from control and MLL-AF9 transplanted mice[11] shipped overnight from S.A.'s laboratory were immediately used upon delivery. BA mice were bred in the presence of 20 mg l^{-1} doxycycline (Sigma-Aldrich, D9891-10G) in their drinking water, and induced for CML-like MPN development by doxycycline withdrawal at 5 weeks of age. Recipient mice were irradiated at a lethal dose of 11 Gy delivered in split doses 3 h apart using a ^{137}Cs source (J. L. Shepherd). BM cells were injected in a volume of 100 µl into the retro-orbital plexus immediately after irradiation, and transplanted mice were treated with antibiotics for 4 weeks post-irradiation. Peripheral blood was obtained from retro-orbital bleeding, and either collected in tubes containing 4 ml of ACK (150 mM NH_4Cl and 10 mM $KHCO_3$) and 10 mM EDTA for flow cytometry analyses, or in EDTA-coated microtainer tubes (Beckton-Dickenson) for complete blood counts using an Hemavet hematology system (Drew Scientific). BM cellularity was determined using a ViCell automated cell counter (Beckman-Coulter). For 5-FU treatments, mice were injected intraperitoneally (i.p.) once with 150 mg kg^{-1} 5-FU (Sigma-Aldrich, F6627-5G) or PBS control. All 5-FU-injected mice were screened for efficient myeloablation by complete blood count analyses and BM cellularity measurement. For Ly-6G treatment, mice were injected i.p. once with 0.1 mg of anti-Ly-6G or rat-IgG control antibodies (UCSF Hybridoma Core Facility). For G-CSF treatments, mice received daily i.p. injections of 5 µg G-CSF (Neupogen) or PBS control. For *Mx1-cre*-mediated deletion, mice were injected i.p. three times 2 days apart with 250 µg of poly(I/C) (pIC, GE Healthcare) in 200 µl PBS. For IL-1β treatments, mice received daily i.p. injections of 0.5 µg IL-1β (Peprotech) or PBS/0.2% BSA control. For megakaryocyte depletion, mice received daily i.p. injections of 250 ng diphtheria toxin (List Biological Laboratories, 150) or PBS control. Megakaryocytes depletion was confirmed by complete blood count analyses and immunofluorescence staining. For proliferation analyses, mice were injected once i.p. with either BrdU (Sigma-Aldrich, B5002-5G) or EdU (Thermo Fisher Scientific, A00144) 1 h before euthanization. For pimonidazol staining, mice were injected with 60 mg kg^{-1} pimonidazole-HCl (Hypoxyprobe, HP2-100Kit) and euthanized 1 h later. For investigations of vascular integrity, mice were injected with 50 µl of dragon green (DG) beads (Bangs Laboratories, FS02F/10597) 10 min before euthanization, and immediately perfused with 10 ml PBS by cardiac puncture before bone collection as described[37]. No specific randomization or blinding protocol was used, mice of both genders were used, and all experiments were performed in accordance with UCSF IACUC approved protocols.

Flow cytometry. BM stem and progenitor populations were analysed and/or isolated as previously described[4]. In brief, BM cells were obtained by either crushing leg, arm and pelvic bones or just flushing leg bones in HBSS containing 2% heat-inactivated FBS (Sigma-Aldrich). HBSS/2% FBS was used for all incubation and wash steps. Erythrocytes and contaminating bone material were removed by ACK lysis followed by centrifugation on a Ficoll gradient (Histopaque 1119, Sigma-Aldrich) for crushed bones. For cell analyses, unfractionated BM cells were incubated with purified, unconjugated-lineage antibodies (CD3 from Biolegend, and CD4, CD5, CD8, B220, Ter119, Mac-1 and Gr-1 from eBioscience) followed by goat anti-rat-PE-Cy5 (Invitrogen, A10691) and subsequently blocked with purified rat IgG (Sigma-Aldrich, I8015-10MG). Cells were then stained with c-Kit-APC-eFluor780 (eBioscience, 47-1171-82), Sca-1-PB (BioLegend, 108120), CD48-A647 (BioLegend, 103416), CD150-PE (BioLegend, 115904) and either CD34-FITC (eBioscience, 11-0341-85) together with FcγR-PerCP-eFluor710 (eBioscience, 46-0161-82) for combined stem/progenitor staining or only ESAM-FITC (Biolegend, 136205) for detailed analyses of HSC and MPP2/3 after 5-FU treatment. For *Csf1r-Gfp* mice, CD34-FITC was replaced by CD34-Bio (Biolegend, 119304) followed by staining with SA-PeCy7 (eBioscience, 25-4317-82). For GMP sorting, BM cells were first pre-enriched for c-Kit$^+$ cells using c-Kit microbeads (Miltenyi Biotec, 130-091-224) and MACS Separation LS Columns (Miltenyi Biotec, 130-042-401), and stained as described with Lin-PE-Cy5, c-Kit-APC-eFluor780, Sca-1-PB, CD34-FITC and FcγR-PerCP-eFluor710. For mature cell analyses, unfractionated BM cells were stained with Mac-1-PE-Cy7 (eBioscience, 25-0112-82), Gr-1-PB (eBioscience, 57-5931-82), B220-APC-Cy7 (eBioscience, 47-0452-82) and CD19-PE (eBioscience, 12-0193-82). Peripheral blood cells were stained with Mac-1-PE-Cy7, Gr-1-PB, B220-APC-Cy7, CD3-APC (eBioscience, 17-0032-82) and Ter119-PE-Cy5 (eBioscience, 15-5921-83), with either co-detection of GFP or addition of CD45.1-FITC (eBioscience, 11-0454-85) and CD45.2-PE (eBioscience, 12-0453) for analyses of chimaeric mice. Stained cells were finally re-suspended in HBSS/2% FBS containing 1 µg ml^{-1} propidium iodide for dead cell exclusion, and either sorted on a FACS ARIAII or analysed on a LSRII using DIVA software (Becton Dickinson). GMPs were double sorted to ensure maximum purity. For intracellular BrdU and Ki67/DAPI staining, BM cells were first stained as above, then fixed in Cytofix/Cytoperm buffer (BD Biosciences, 554714) for 10 min (BrdU) or 30 min (Ki67/DAPI) in the dark, washed in PermWash (BD Biosciences), permeabilized with CytoPerm Plus (BD Biosciences) for 10 min at room temperature, re-fixed in Cytofix/Cytoperm buffer for 5 min in the dark and washed in PermWash. For BrdU staining, cells were then treated with 0.5 U µl^{-1} DNaseI in 3% BSA, 0.2× PBS, 5 mM $MgCl_2$ and 2 mM $CaCl_2$ for 30 min at room temperature in the dark, washed in PermWash, stained with FITC-conjugated anti-BrdU (347583, BD Biosciences) for 30 min at room temperature, washed in PermWash, and re-suspended in HBSS/2% FBS. For Ki67/DAPI staining, cells were then stained with anti-Ki67 antibody (eBioscience, 11-5698-80) for 1 h at room temperature in the dark, washed in PermWash and re-suspended in HBSS/2% FBS containing DAPI at 1 µg ml^{-1} (Sigma-Aldrich, 32670). In both cases, cells were analysed on a FACS LSR II as described above.

Immunofluorescence on tissue sections. Mouse femurs or spleens were snap frozen in OCT (Tissue-Tek) and kept at −80 °C until sectioning. Frozen samples were cryosectioned (7 µm) using a Cryostat equipped with the Cryojane tape transfer system and tungsten blades (Leica Microsystems). Sections were dried for 2–4 h at room temperature and then frozen at −80 °C until stained. Before staining, sections were fixed with 100% acetone for 10 min at −20 °C, dried for 5 min at room temperature and blocked for 1 h 30 min with 10% goat-serum (Gibco) in PBS. For regular GMP staining, sections were incubated first with rat anti-mouse c-Kit (Biolegend, 135102) primary antibody overnight at 4 °C in PBS/10% goat-serum, followed with a goat anti-rat-Cy3 (Jackson Immunoresearch, 112-165-167) secondary antibody for 1 h at room temperature in PBS/10% goat-serum and washed three times for 5 min with PBS at room temperature. These wash steps were also performed between each staining steps. Sections were then blocked with 20 µg ml^{-1} Rat IgG (Sigma-Aldrich, I8015-10MG) for 10 min at room temperature in PBS, and finally stained with A488-conjugated lineage markers (B220 from Invitrogen, and Mac-1, Gr-1 and CD3 from Biolegend), Sca-1-A488 (Biolegend, 108116), CD150-A488 (Biolegend, 115916) and FcγR-A647 (UCSF Hybridoma Core Facility) for 1 h 30 min at room temperaturein PBS/10% goat-serum. For GMP staining of the MLL-AF9 transplantation model, the eBioscience mouse haematopoietic lineage biotin panel (88-7774), Sca-1-bio (eBioscience, 13-5981-1630), and CD150-bio (Biolegend, 115908) were used instead of A488-conjugated antibodies, followed by staining with a SA-e450 (eBioscience, 48-4317) antibody. For laminin and GMP co-staining, FcγR was omitted and rabbit anti-mouse laminin (Sigma-Aldrich, L9393) followed by staining with a goat anti-rabbit-A647 secondary antibody was used instead. For the other GMP co-staining, A647-conjugated lineage antibodies (Biolegend, B220, Mac-1, Gr-1 and CD3), Sca-1-A647 (Biolegend, 108118) and CD150-A647 (Biolegend, 115918) were used instead of A488-conjugated antibodies, and FcγR was omitted. For laminin and extracellular matrix protein co-detection, rabbit anti-mouse laminin, Collagen IV (Abcam, ab6586) and fibronectin (Abcam, ab23750) were used followed by staining with a donkey anti-rabbit-A488 (Sigma-Aldrich, A-21206) secondary antibody. For clonality analyses, either CD45.2-FITC (Biolegend, 109816) or A488-conjugated anti-GFP (Aves labs, GFP-1020) were used. For laminin and DG-bead co-staining, sections were just stained with rabbit anti-mouse laminin followed by goat anti-rabbit-A647. For proliferation analyses, either pH3-FITC (Cell Signaling, 9708S) or Click-iT EdU Alexa Fluor 488 Imaging Kit (ThermoFisher Scientific, C10337) were used according to the manufacturer's instructions. For myeloid/lymphoid cells and GMP co-staining, FcγR, CD150 and Sca-1 were omitted and B220-A488 (Invitrogen, RM2620), CD3-A488 (Biolegend, 100210), Gr-1-A647 (Biolegend, 108418) and Mac-1-A647 (Biolegend, 101218) were used instead. For megakaryocytes and GMP co-staining, FcγR was omitted and rat anti-mouse CD150 (Biolegend, 115902) followed by staining with a goat anti-rat-Cy3 secondary antibody was used instead. For cleaved caspase 3 (CC3) and GMP co-staining, FcγR was omitted and sections were fixed for 10 min with 4% PFA at room temperature then washed three times for 5 min at room temperature in PBS/0.1% Triton X-100. Sections were first incubated with a rabbit anti-CC3 (Cell Signaling, 9661-S) antibody followed by a goat anti-rabbit-A647 (Thermo Fisher Scientific, A-21245) secondary antibody, and then stained as usual for c-Kit and A488-conjugated lineage. For pimonidazol staining, frozen sections were fixed with 4% PFA for 10 min at room temperature and stained with FITC-conjugated anti-pimonidazole (Hypoxyprobe, HP2-100Kit) according to the manufacturer's instructions. After staining, all sections were counterstained with 1 µg ml^{-1} DAPI in PBS for 10 min at room temperature, mounted with fluoromount (Southern Biotech, 0100-01) and imaged on SP5 upright or SP8 inverted confocal microscopes (Leica) with a 20× objective. Images were processed using Volocity software (Perkin Elmer v.6.2) and

analysed with ImageJ. The analyse particle function and a threshold mask covering laminin$^+$ cells was also used in ImageJ to quantify dragon-green bead mean fluorescence intensity outside of blood vessels.

Immunofluorescence on purified cells. GMP (2,000 cells per slide) were directly sorted onto poly-lysine coated slides (Sigma-Aldrich, P0425-72EA) and allowed to settle for 15 min. Cells were washed three times for 5 min with PBS between each staining step. For GMP re-stain, cells were fixed with 100% acetone for 5 min at −20 °C, blocked for 1 h 30 min at room temperature with PBS/10% goat serum and stained as described above for regular GMP staining on sections. For β-catenin staining, cells were fixed with 4% PFA for 10 min at room temperature, and then permeabilized and blocked with PBS/0.1% Tween-20/10% FBS for 1 h. Cells were then stained with a rabbit anti-mouse β-catenin (Cell Signaling, 9582S) primary antibody overnight at 4 °C in PBS/0.1% Tween-20/10% FBS, followed by an anti-rabbit-A555 (Invitrogen, A31572) secondary antibody for 1 h at room temperature in PBS/0.1% Tween-20/10% FBS. Slides were mounted with VectaShield (Vector Laboratories, H-1200) containing 1 μg ml^{-1} DAPI and imaged on a SP5 upright confocal microscope (Leica) with a 20× objective. Images were processed using Volocity software and an average of 390 individual cells were scored per condition for nuclear β-catenin quantification.

***In vitro* analyses.** All cultures were performed at 37 °C in a 5% CO_2 water jacket incubator (Thermo Scientific). For clonogenic methylcellulose colony assays, GMPs (1 cell per well) were directly sorted into 96-well plates containing 100 μl methylcellulose (Stem Cell Technologies, M3231) supplemented with the following cytokines (all from PeproTech): IL-3 (10 ng ml^{-1}), GM-CSF (10 ng ml^{-1}), SCF (10 ng ml^{-1}), IL-11 (10 ng ml^{-1}), Flt-3L (10 ng ml^{-1}), Tpo (100 ng ml^{-1}) and Epo (4 U ml^{-1}). Colonies were visually scored after 7 days of culture.

Fluidigm analyses. Gene expression analyses using the Fluidigm 96.96 Dynamic Array IFC were performed as previously described[4]. Briefly, GMPs (100 cells per well) were directly sorted into 96 well-plates containing CellsDirect lysis buffer (Invitrogen, 11753-100), reverse-transcribed and pre-amplified for 18 cycles using Superscript III Platinum Taq DNA polymerase (Invitrogen, 18080-044) using a custom-made set of 96 proprietary target-specific primers (Fluidigm). The resulting cDNAs were analysed on a Biomark system (Fluidigm) using EvaGreen Sybr dye (Bio-Rad, 172-5211). Data were collected using Biomark Data Collection Software (Fluidigm) and analysed using Biomark qPCR analysis software with a quality threshold of 0.65 and linear baseline correction. Identical settings were used across all experiments performed on different 96.96 dynamic arrays. Melt curves and T_m values for each assay reaction were checked individually, and reactions with melt curves showing multiple peaks or poor quality (<0.65) were discarded, leaving 60 genes and 2 housekeeping genes (*Gusb* and *Gapdh*) for further analyses. For gene expression quantification, data were exported as an Excel.csv file and analysed by the $\Delta\Delta C_t$ method using *Gusb* (5-FU GMPs) or *Gapdh* (MPN GMPs) for normalization. tSNE and principal component analyses were performed as previously described[4] on the 59 (5-FU GMPs) and 35 (MPN GMPs) most robustly expressed genes following quality control assessment, and normalized to *Gapdh*.

Single-cell RNA-seq. Single GMPs were directly sorted into individual wells of a 96-well PCR plate containing 2.3 μl of 0.2% Triton X-100 (Sigma-Aldrich, 93443) and 2.3 U of SUPERase-In RNase Inhibitor (Ambion, AM2694). cDNA was obtained and amplified following the described SMARTSEQ2 protocol[38]. Libraries were prepared for sequencing from 125 ng of cDNA using the Illumina Nextera XT DNA preparation kit. Pooled libraries were run on the Illumina HiSeq 2500 (5-FU samples) or Illumina HiSeq 4000 (BA samples). Reads were mapped to the *Mus musculus* genome (Ensembl GRCm38.81) and the ERCC sequences using GSNAP (version 2015-09-29) with -B 5 (batch mode 5) -n 1 (maximum pathsallowed: 1) -Q (if maximum paths more than n, not print) -N 1 (look for novel splicing). HTseq-count was used to count the number of reads mapped to each gene with -s no (non-strand specific mode)[39]. For further analyses, we only retained samples that had (1) more than 100,000 reads mapped to nuclear mRNAs; (2) more than 4,000 highly detectable genes (defined as genes with more than 10 reads per million); and (3) less than 20% of mapped reads allocated to mitochondrial genes. The data were normalized for sequencing depth using the package scran from R Bioconductor. Highly variable genes were identified as described[40], using a false discovery rate threshold equal to 0.1. Only highly variable genes were considered to perform principal component analysis, using the prcomp command in R. Hierarchical clustering was performed using highly variable genes to identify ssGMPs and srGMPs. The pairwise Spearman correlation coefficients (ρ) were calculated between the expression levels of highly variable genes in each pair of cells. The dissimilarity matrix was then calculated as $(1-\rho)/2$. Hierarchical clustering was performed using the default 'complete' method on the dissimilarity matrix. Identification of cells contained in each of the two clusters (corresponding to ssGMPs and srGMPs) was done using the cutree method with k = 2 (2 groups). Genes differentially expressed (DE) between ssGMP and srGMP clusters were identified using DESeq2 (version 1.12.2)[41] and only DE genes having a fold change significantly greater than 1.5 with a false discovery rate threshold less than 0.1 were used for hierarchical clustering.

qRT–PCR. For megakaryocytes enrichment, flushed BM cells were filtered through a 100-μm mesh filter and sedimented 30 min at room temperature through a gradient of 1.5 to 3% BSA, with megakaryocytes pelleting at the bottom of the 3% BSA gradient. Total RNA was isolated from 3×10^4 cells re-suspended in Trizol LS (Life Technologies, 10296-010) according to the manufacturer's protocol. For qRT–PCR, RNA was treated with DNaseI and reverse-transcribed using SuperScript III kit and random hexamers (Life Technologies, 18080-051). Runs were performed on a 7900HT Fast Real-Time PCR system (Applied Biosystems) using SybrGreen reagents (Kapa Biosystems, KK4603) and the cDNA equivalent of 200 cells per reaction. Sequences for qRT–PCR primers were: *Cxcl4* sense 5′-TCTCCTCTGGGATCCATCTT-3′, *Cxcl4* antisense 5′-CATTCTTCAGGGTGGCTATGA-3′ (NM_019932); *Actb* sense 5′-GACGGCCAGGTCATCACTATTG-3′, *Actb* antisense 5′-AGGAAGGCTGGAAAAGAGCC-3′ (NM_007393). Values were normalized to *Actb* expression levels.

Cytokine ELISA. For collecting BM fluids, the four long bones (two femurs and two tibiae) of each mouse were flushed with the same 200 μl of HBSS/2% FBS using a 0.3cc insulin syringe with a 28g needle and spun at 500*g* for 5 min to remove BM cells. Supernatants were further clarified by spinning down at 12,000*g* for 10 min, and samples were subsequently stored at −80 °C until use. For ELISA measurements, 4×-diluted (SCF, CXCL12, FGF1), 5×-diluted (TGFβ1), 20×-diluted (G-CSF) and 1,000×-diluted (CXCL4) samples were analysed according to the manufacturer's instructions (Raybiotech for SCF, G-CSF, CXCL4 and CXCL12; R&D Systems for TGFβ1) or as previously described for FGF1 (ref. 22).

Statistics. All experiments were repeated as indicated. *n* indicates the numbers of independent biological repeats. The numbers of independent experiments are reported in the Supplementary Information. For immunofluorescence images, representative examples of at least two independent experiments are shown. Data are expressed as means ± s.d. unless otherwise indicated. Statistical analyses were performed using Prism 5.0 software (GraphPad). Pairwise statistical significance was evaluated by Student's *t*-test. Mice for treatment and transplantation were randomized, and no blinding protocol was used. No statistical method was used to predetermine sample size. $P \leq 0.05$ was considered statistically significant.

Data availability. Datasets that support the findings of this study have been deposited online with the Gene Expression Omnibus (GEO) under accession number GSE90799. Source Data for all the figures are provided with the paper. All other data are available from the corresponding author upon reasonable request.

29. Glaccum, M. B. *et al.* Phenotypic and functional characterization of mice that lack the type I receptor for IL-1. *J. Immunol.* **159,** 3364–3371 (1997).
30. Sasmono, R. T. *et al.* A macrophage colony-stimulating factor receptor-green fluorescent protein transgene is expressed throughout the mononuclear phagocyte system of the mouse. *Blood* **101,** 1155–1163 (2003).
31. Wright, D. E. *et al.* Cyclophosphamide/granulocyte colony-stimulating factor causes selective mobilization of bone marrow hematopoietic stem cells into the blood after M phase of the cell cycle. *Blood* **97,** 2278–2285 (2001).
32. Brault, V. *et al.* Inactivation of the β-catenin gene by Wnt1-Cre-mediated deletion results in dramatic brain malformation and failure of craniofacial development. *Development* **128,** 1253–1264 (2001).
33. Harada, N. *et al.* Intestinal polyposis in mice with a dominant stable mutation of the β-catenin gene. *EMBO J.* **18,** 5931–5942 (1999).
34. Kühn, R., Schwenk, F., Aguet, M. & Rajewsky, K. Inducible gene targeting in mice. *Science* **269,** 1427–1429 (1995).
35. Tiedt, R., Schomber, T., Hao-Shen, H. & Skoda, R. C. *Pf4-Cre* transgenic mice allow the generation of lineage-restricted gene knockouts for studying megakaryocyte and platelet function *in vivo*. *Blood* **109,** 1503–1506 (2007).
36. Buch, T. *et al.* A Cre-inducible diphtheria toxin receptor mediates cell lineage ablation after toxin administration. *Nat. Methods* **2,** 419–426 (2005).
37. Fuxe, J. *et al.* Pericyte requirement for anti-leak action of angiopoietin-1 and vascular remodeling in sustained inflammation. *Am. J. Pathol.* **178,** 2897–2909 (2011).
38. Picelli, S. *et al.* Full-length RNA-seq from single cells using Smart-seq2. *Nat. Protocols* **9,** 171–181 (2014).
39. Anders, S., Pyl, P. T. & Huber, W. HTSeq--a Python framework to work with high-throughput sequencing data. *Bioinformatics* **31,** 166–169 (2015).
40. Brennecke, P. *et al.* Accounting for technical noise in single-cell RNA-seq experiments. *Nat. Methods* **10,** 1093–1095 (2013).
41. Love, M. I., Huber, W. & Anders, S. Moderated estimation of fold change and dispersion for RNA-seq data with DESeq2. *Genome Biol.* **15,** 550 (2014).

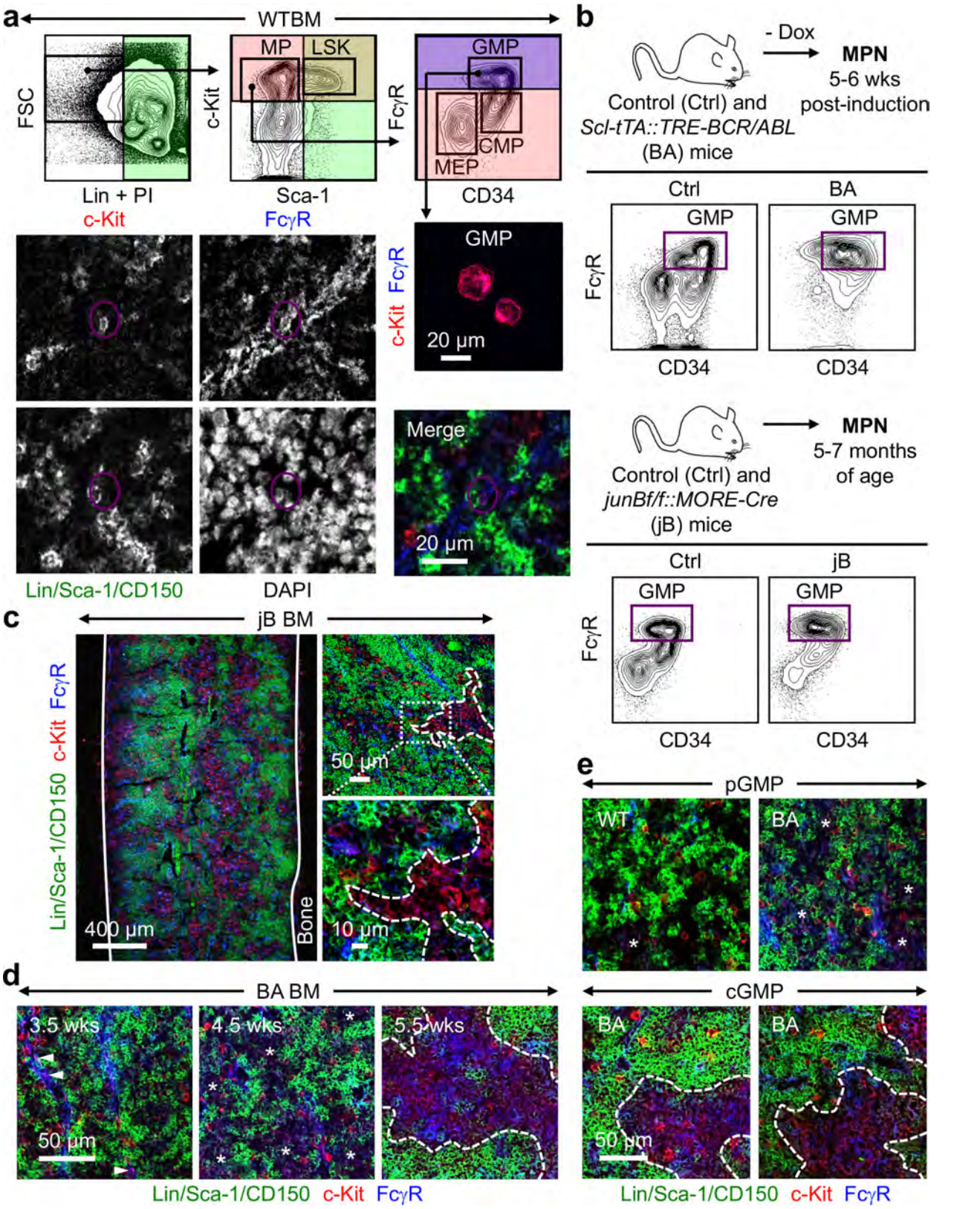

Extended Data Figure 1 | Imaging GMPs in normal and leukaemic conditions. a, Gating strategy used to identify GMPs showing representative FACS plots with purified GMPs (purple) stained with immunofluorescence markers, and a representative wild-type GMP (purple circle) on bone section. **b**, Inducible BA and constitutive jB mouse models of human MPN with representative GMP FACS plots. Dox, doxycycline. **c**, Representative immunofluorescence staining showing GMPs (purple) in the BM of diseased jB mice. **d**, Progression of cGMP formation with disease development in BA mice at the indicated weeks after withdrawal of doxycycline. **e**, Representative examples of loose pGMPs and compact cGMPs in wild-type and BA mice. Solid lines indicate bone surface; dotted lines denote cGMPs and stars indicate pGMPs.

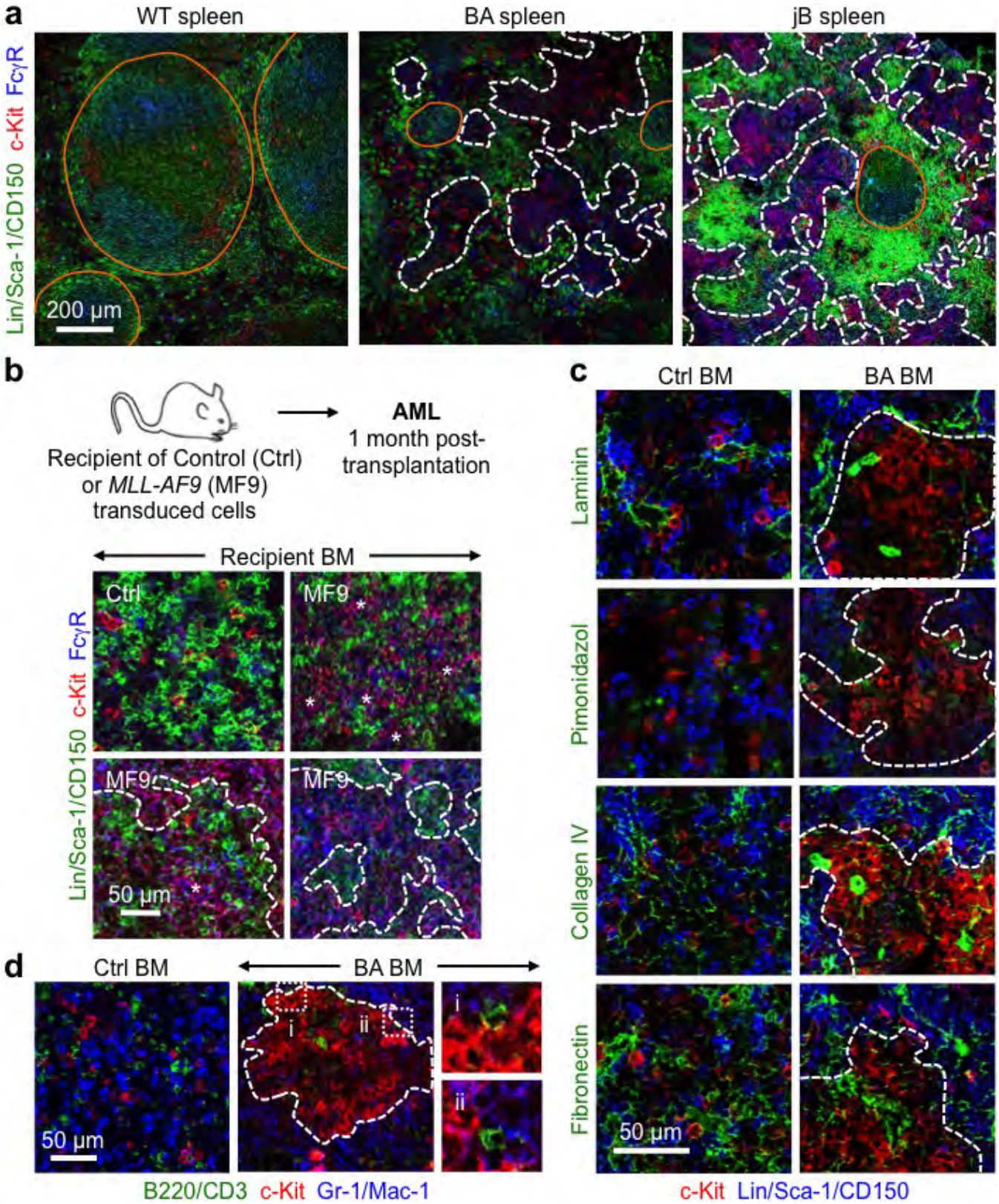

Extended Data Figure 2 | GMP cluster features. a, Representative immunofluorescence staining of GMPs (purple) in spleens from wild-type and diseased BA and jB mice. **b**, cGMPs in recipient mice developing AML after transplantation of MLL-AF9 (MF9)-transduced LSK-derived cells. Experimental scheme and representative immunofluorescence staining of GMPs (purple) in BM from control and diseased MF9 recipient mice. Three individual recipient mice are shown for MF9. **c**, Representative immunofluorescence staining showing myeloid progenitors (red) in relation to the indicated stromal features (green) in BM from control and diseased BA mice. **d**, Representative immunofluorescence staining showing myeloid progenitors (red) in relation to mature lymphoid (green) and myeloid (blue) cells in BM from control and diseased BA mice. **i** and **ii** highlight two magnified areas. Orange lines indicate germinal centre; arrowheads denote individual GMPs; stars indicate pGMPs and dotted lines denote cGMPs.

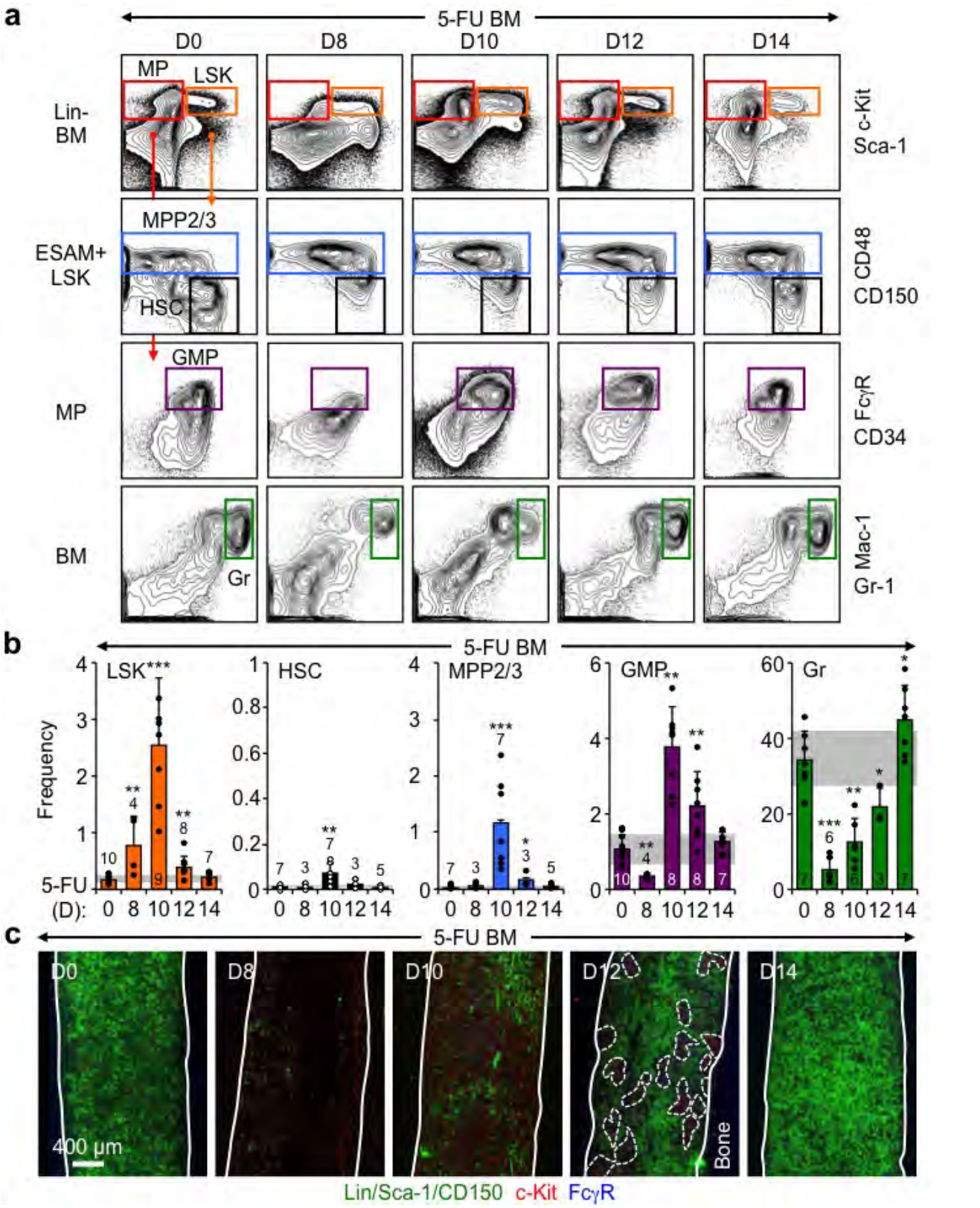

Extended Data Figure 3 | Regenerating BM after 5-FU treatment. **a**, Gating strategy used to identify the indicated BM populations by flow cytometry in 5-FU-treated wild-type mice. Representative FACS plots are shown at the indicated days after treatment. **b**, Frequency of BM LSK cells, HSCs, MPP2/MPP3, GMPs and granulocytes at the indicated days after 5-FU treatment. **c**, Representative immunofluorescence staining showing GMPs (purple) in BM from 5-FU treated mice at the indicated days after treatment. Of note, cGMPs were observed in all investigated bones (that is, femur, tibia, humerus and sternum) at day 12 after 5-FU treatment. Solid lines indicate bone surface; dotted lines denote cGMPs. Data are mean ± s.d. (grey bars, reference range); $*P \leq 0.05$, $**P < 0.01$, $***P < 0.001$ (Student's *t*-test).

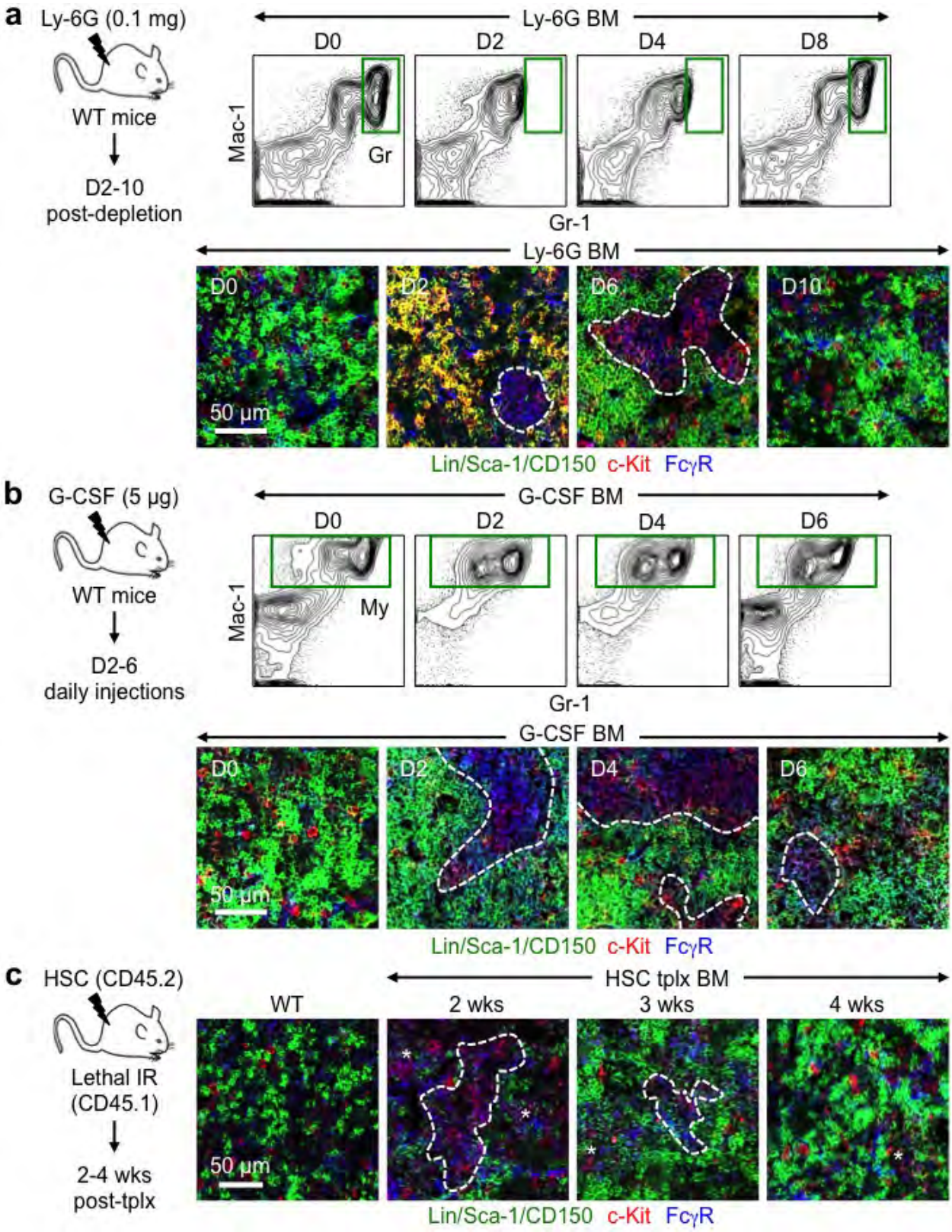

Extended Data Figure 4 | GMP clusters during myeloid regeneration and expansion. a, Granulocyte depletion in the BM of Ly-6G-treated mice, with experimental scheme (top left), representative FACS plots (top right) and immunofluorescence staining of GMPs (purple) (bottom) at the indicated days after treatment. **b**, Granulocyte expansion in the BM of G-CSF-treated mice, with experimental scheme (top left), representative FACS plots (top right) and immunofluorescence staining of GMPs (purple) (bottom) at the indicated days after treatment. **c**, GMP clusters in the BM of HSC-transplanted mice, with experimental scheme (left) and representative immunofluorescence staining of GMPs (purple) at the indicated weeks after transplantation (right). Non-transplanted wild-type BM is shown for comparison; IR, ionizing radiation. Stars indicate pGMPs and dotted lines denote cGMPs.

a

	% CD45.2 chimera BM										
	D0		D8		D10		D12			D14	
	(a)	(b)	(a)	(b)	(a)	(b)	(a)	(b)	(c)	(a)	(b)
Pre 5-FU (PB)	24%	24%	21%	24%	26%	24%	29%	22%	26%	30%	30%
Post 5-FU (BM)	16%	20%	46%	19%	17%	8%	28%	10%	67%	36%	33%

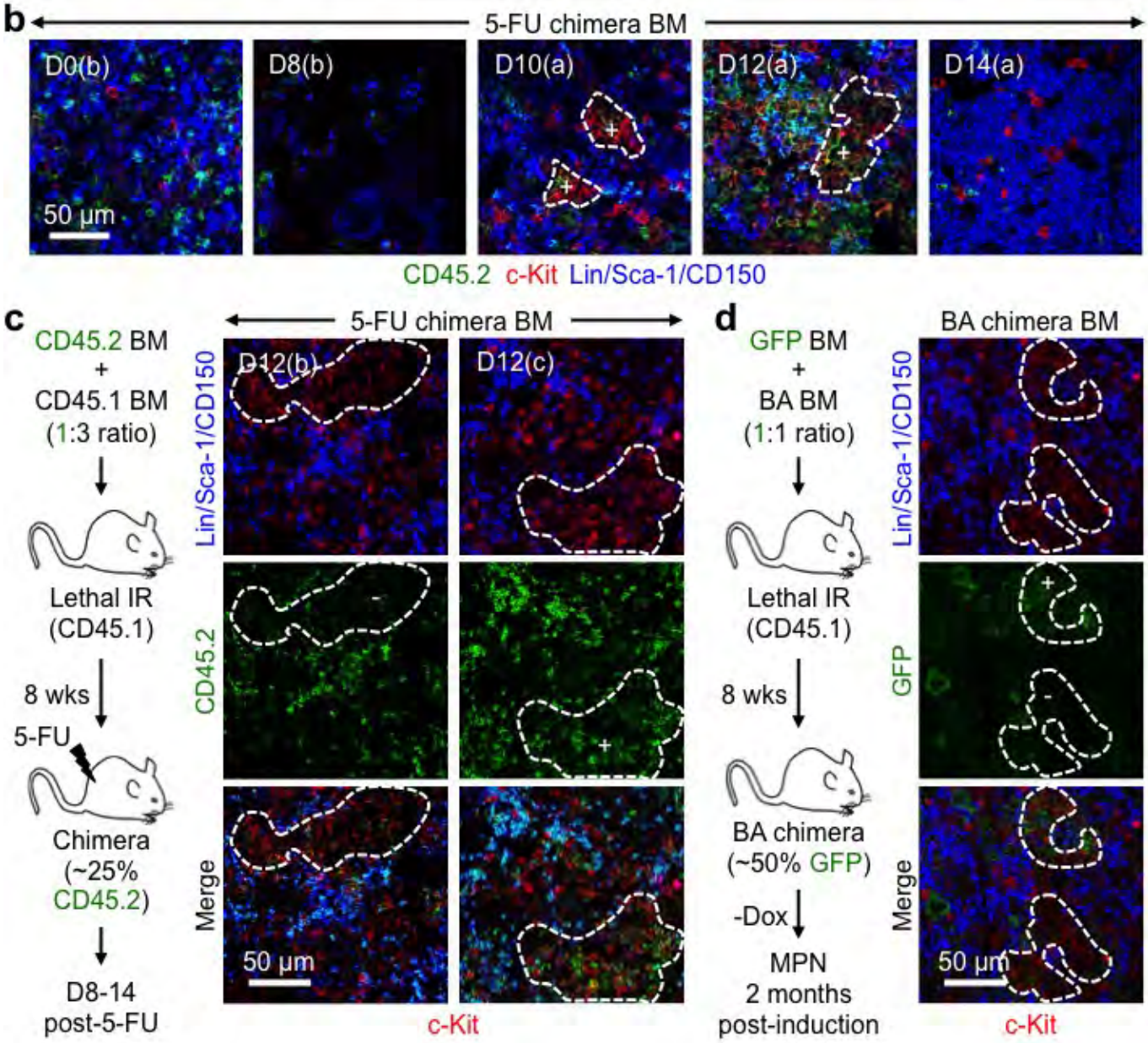

Extended Data Figure 5 | GMP clusters are clonal. a–**c**, Clonality of regenerative GMP clusters. **a**, Percentage of CD45.2$^+$ cells in the peripheral blood (PB) pre-treatment and the BM after 5-FU treatment for each of the chimaera mice used at the indicated days after 5-FU treatment. **b**, Representative immunofluorescence staining showing myeloid progenitors (red) and CD45.2 (green) expression in BM from 5-FU-treated chimaera mice at the indicated days after treatment. **c**, Experimental scheme (left) and representative immunofluorescence staining (right) showing myeloid progenitors (red) and CD45.2 (green) expression separately in BM from two independent day 12 5-FU-treated chimaera mice. Positive (+) clusters have ≥75% CD45.2$^+$ cells and negative (−) clusters ≤5% CD45.2$^+$ cells. **d**, Clonality of leukaemic GMP clusters with experimental scheme (left) and representative immunofluorescence staining (right) showing myeloid progenitors (red) and GFP (green) expression from *Actb-Gfp* cells in BM from diseased BA chimaera mice. Positive (+) clusters have ≥75% GFP$^+$ cells and negative (−) clusters ≤5% GFP$^+$ cells. Dotted lines denote cGMPs.

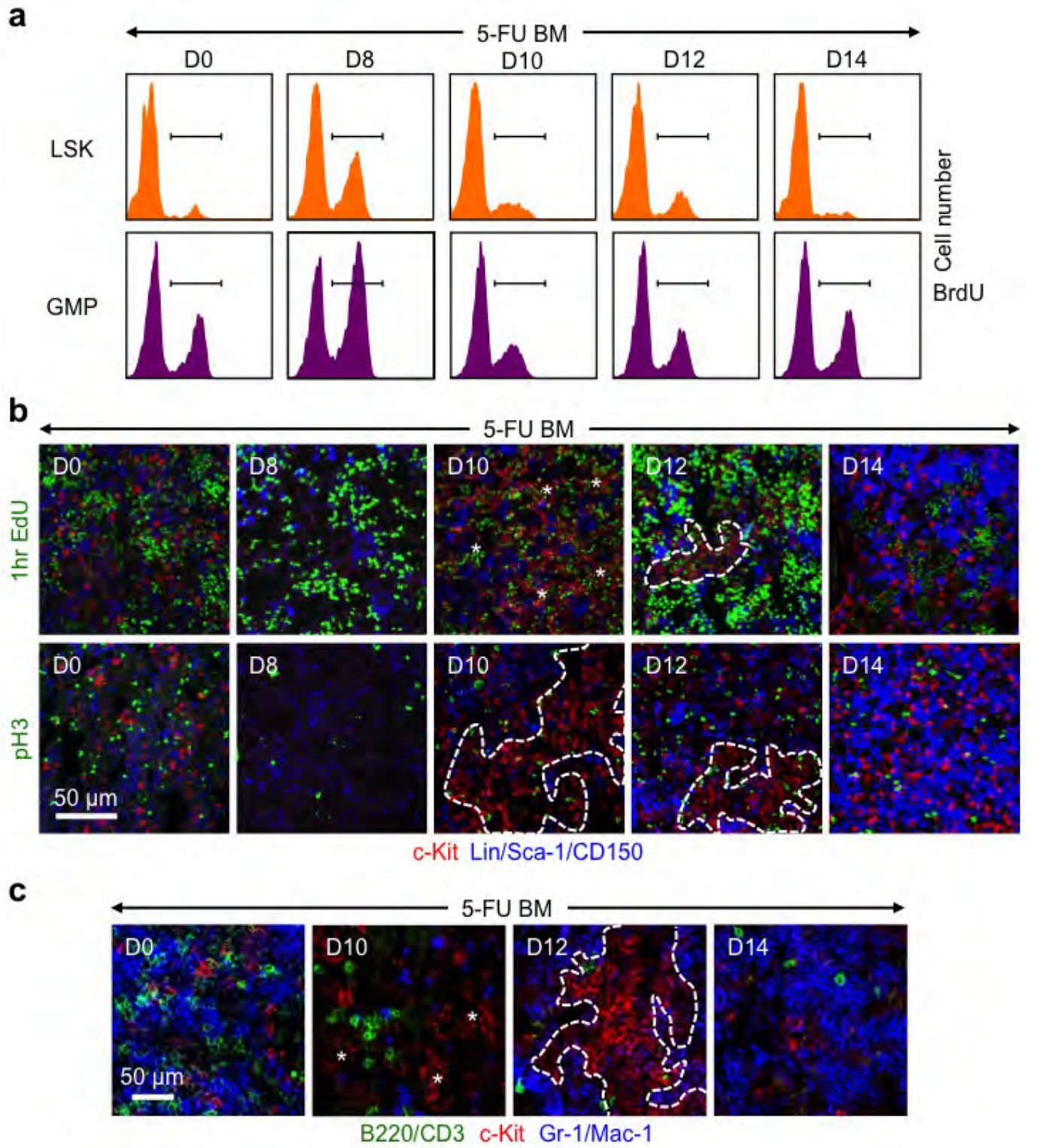

Extended Data Figure 6 | Dynamic proliferation and differentiation in regenerating GMP clusters. a, Representative FACS plots showing kinetics of BrdU incorporation in LSKs and GMPs from 5-FU-treated wild-type mice at the indicated days after treatment. **b**, Representative immunofluorescence staining showing myeloid progenitors (red) in relation to proliferating EdU^+ (green, top row) and dividing $pH3^+$ (green, bottom row) cells in BM from 5-FU-treated wild-type mice at the indicated days after treatment. **c**, Representative immunofluorescence staining showing myeloid progenitors (red) in relation to mature lymphoid (green) and myeloid (blue) cells in BM from 5-FU-treated wild-type mice at the indicated days after treatment. Stars indicate pGMPs and dotted lines denote cGMPs.

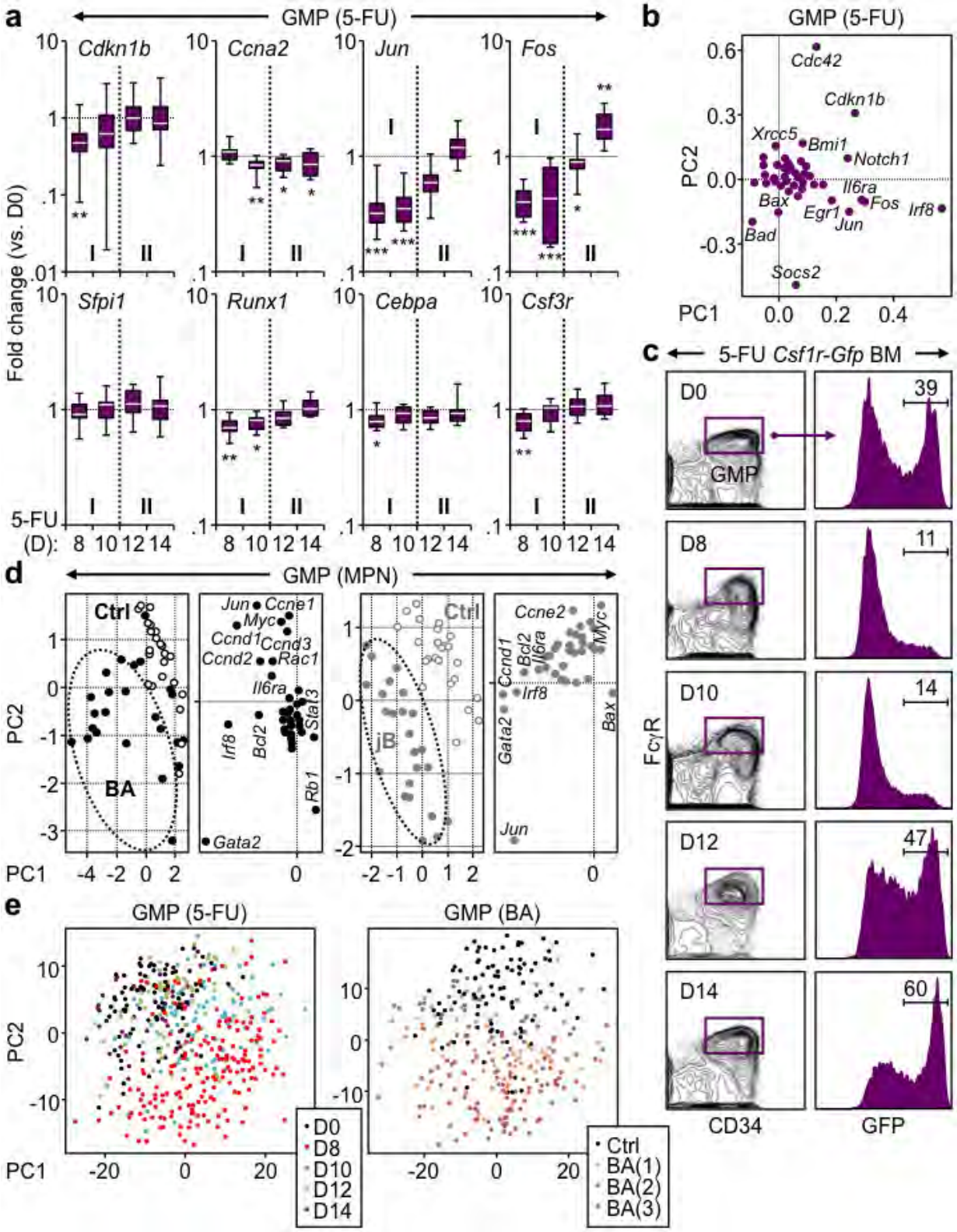

Extended Data Figure 7 | Molecular reprogramming in regenerating and leukaemic GMP clusters. a, Additional Fluidigm gene expression analyses of regenerating GMPs isolated from 5-FU-treated wild-type mice at the indicated days after treatment ($n = 2$; 10–16 pools of 100 cells per condition). Results are expressed as fold change compared to levels in untreated (D0) GMPs and presented as boxplots (line: median; box: twenty-fifth and seventy-fifth percentiles; whisker: ninetieth and tenth percentiles). **b**, Loading association of principal component analyses of Fluidigm gene expression data from regenerating GMPs. **c**, Representative FACS plots of GFP expression in GMPs of 5-FU-treated *Csf1r-Gfp* reporter mice at the indicated days after treatment. **d**, tSNE analyses and loading association of principal component analyses of Fluidigm gene expression data from MPN GMPs isolated from diseased BA, jB and respective age-matched control mice ($n = 4$; 22–28 pools of 100 cells per condition). **e**, Principal component analyses of single-cell GMP RNA-seq data showing the distribution of each 5-FU-treatment time point (day 0: 89 cells; day 8: 187 cells; day 10: 89 cells; day 12: 75 cells; day 14: 36 cells) and individual control (94 cells) and BA (BA(1): 68 cells; BA(2): 57 cells; BA(3): 87 cells) mice. $*P \leq 0.05$, $**P \leq 0.01$, $***P \leq 0.001$ (Student's *t*-test).

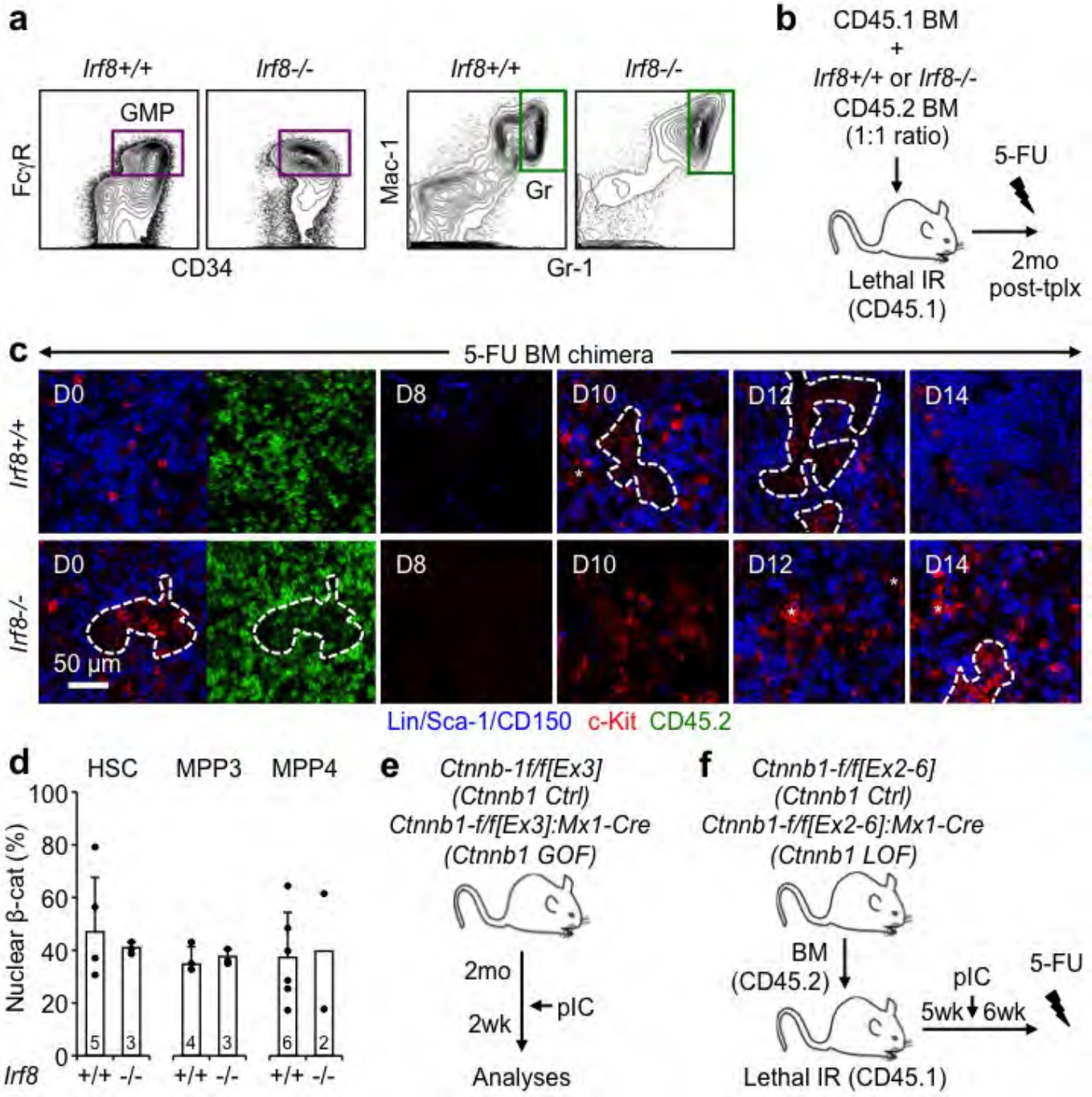

Extended Data Figure 8 | *Irf8* and *Ctnnb1* function in self-renewing GMPs. a, Representative FACS plots showing GMPs and granulocytes at the steady state in *Irf8*$^{+/+}$ and *Irf8*$^{-/-}$ mice. **b**, Experimental scheme for BM from *Irf8*$^{+/+}$ and *Irf8*$^{-/-}$ chimaeric mice. **c**, Representative immunofluorescence staining of donor-derived CD45.2^{+} (green) myeloid progenitors (red) in BM from 5-FU-treated *Irf8*$^{+/+}$ and *Irf8*$^{-/-}$ chimaeric mice. **d**, Nuclear β-catenin expression in HSCs, and MPP3 and MPP4 populations from *Irf8*$^{+/+}$ and *Irf8*$^{-/-}$ mice. Results are expressed as the percentage of positive cells. **e**, **f**, Experimental scheme for *Ctnnb1* control and *Ctnnb1* LOF (**e**) or *Ctnnb1* (GOF) (**f**) mice. Stars indicate pGMPs and dotted lines denote cGMPs. Data are mean ± s.d.

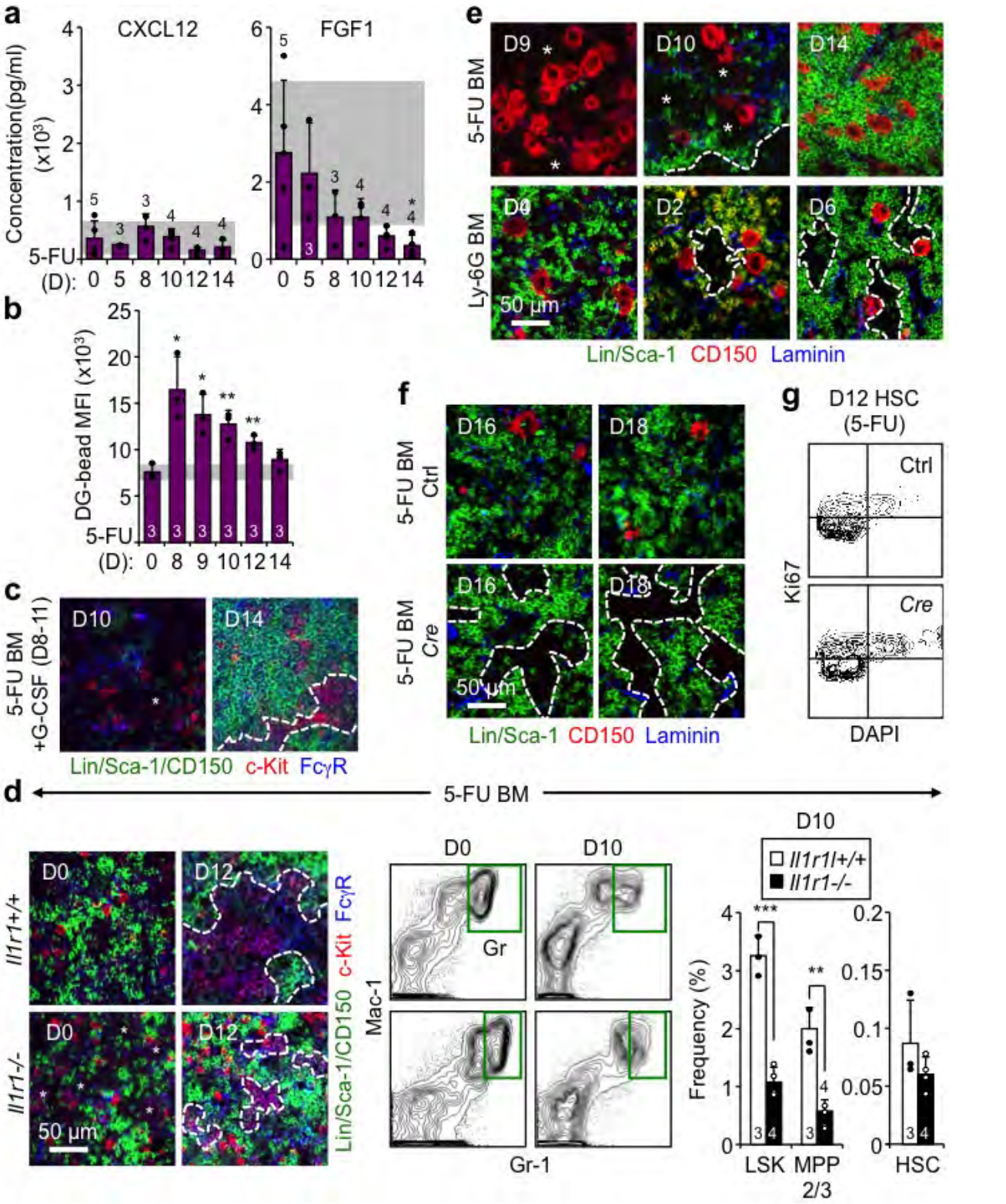

Extended Data Figure 9 | Mechanisms controlling GMP cluster formation during regeneration. a, ELISA measurement of cytokine levels in BM fluids of 5-FU-treated wild-type mice at the indicated days after treatment ($n = 3$). **b**, Quantification of vascular leakage in 5-FU-treated BM at the indicated days after treatment ($n = 3$). Results are expressed as dragon-green (DG) bead mean fluorescence intensity (MFI) upon masking of laminin$^+$ blood vessels. **c**, Representative immunofluorescence staining showing GMPs (purple) in BM from 5-FU-treated mice with concomitant daily injections of G-CSF on days 8 to 11. **d**, Investigation of 5-FU-treated *Il1r1*$^{+/+}$ and *Il1r1*$^{-/-}$ mice at the indicated days after treatment showing representative immunofluorescence staining of GMPs (purple) (left), FACS plots of granulocyte regeneration (middle), and quantification of the indicated BM populations (right). **e**, Representative immunofluorescence staining of CD150$^+$ megakaryocytes (red) in BM from 5-FU- and Ly-6G-treated mice. **f**, **g**, Megakaryocyte depletion studies in diphtheria toxin-injected *iDtr* (control) and *Cxcl4-cre:iDtr* (*cre*) mice showing representative immunofluorescence staining of CD150$^+$ megakaryocytes (red) at the indicated days after 5-FU treatment (**f**), and representative Ki67 and DAPI staining of HSCs at day 12 (**g**). Stars indicate pGMPs and dotted lines denote cGMPs. Data are mean ± s.d. (grey bars, reference range); $^*P \leq 0.05$; $^{**}P \leq 0.01$, $^{***}P \leq 0.001$ (Student's *t*-test).

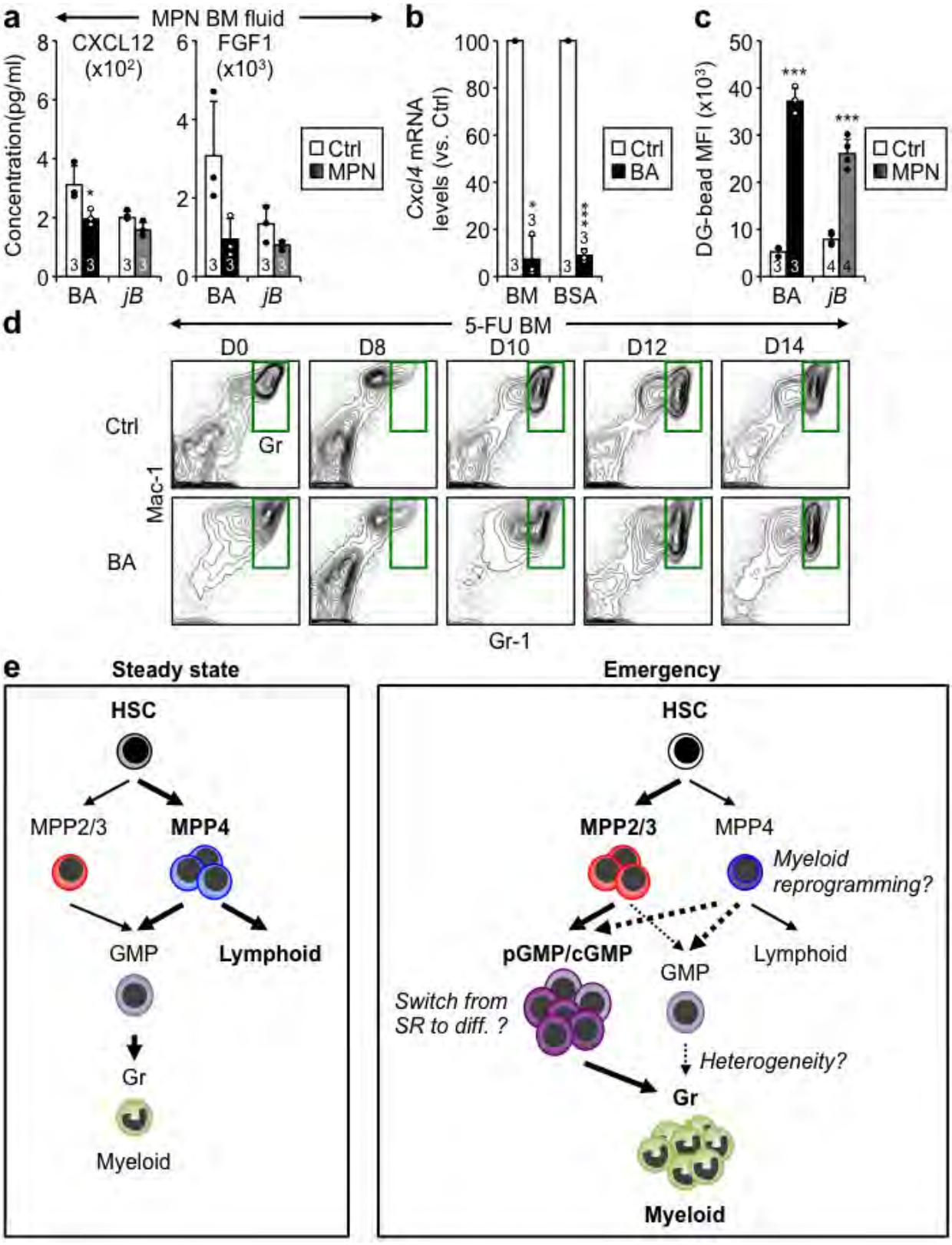

Extended Data Figure 10 | See next page for caption.

Extended Data Figure 10 | Deregulated GMP cluster formation in leukaemic mice. a, ELISA measurements of cytokine levels in BM fluids of BA, jB and respective control mice ($n = 3$). **b**, qRT–PCR measurement of *Cxcl4* expression in BM and megakaryocyte-enriched BSA gradient of control and BA mice ($n = 3$). **c**, Quantification of vascular leakage in diseased BA ($n = 3$) and jB ($n = 3$) mice. Results are quantified as dragon-green (DG) bead mean fluorescence intensity upon masking of laminin$^+$ blood vessels. **d**, Representative FACS plots showing granulocyte regeneration in 5-FU-treated control and BA mice at the indicated days after treatment. **e**, Revised model of emergency myelopoiesis. At the steady state, blood production reflects the differential generation by HSCs of a small number of myeloid-biased MPP2/MPP3 and a large number of lymphoid-biased MPP4 subsets, which both give rise to GMPs and contribute to myeloid output. By contrast, in emergency situations, HSCs are induced to overproduce MPP2/MPP3, and MPP4 are reprogrammed towards almost exclusive myeloid output, in large part due to cytokine stimulations and the triggering of specific regulatory pathways. An important consequence of the activation of this myeloid regeneration axis is the generation of localized pGMP/cGMP differentiation foci in the BM cavity, which drive the granulocyte production. This entire process is tightly regulated by BM niche signals and is transient during emergency myelopoiesis, but is constantly activated in myeloid leukaemia. Important emerging questions are what controls the switch from self-renewing pGMP to differentiating cGMP clusters, if myeloid-reprogrammed MPP4 also generate pGMP/cGMPs and expanded MPP2/MPP3 continue to produce regular GMPs (dotted lines), and whether granulocytes produced through this regeneration axis functionally differ from steady-state granulocytes (heterogeneity). Data are mean ± s.d. $*P \leq 0.05$, $***P \leq 0.001$ (Student's *t*-test).